NASA/TM—2004-213066

Detailed Microstructural Characterization of the Disk Alloy ME3

Timothy P. Gabb
Glenn Research Center, Cleveland, Ohio

Anita Garg
University of Toledo, Ohio

David L. Ellis and Kenneth M. O'Connor
Glenn Research Center, Cleveland, Ohio

May 2004

The NASA STI Program Office . . . in Profile

Since its founding, NASA has been dedicated to the advancement of aeronautics and space science. The NASA Scientific and Technical Information (STI) Program Office plays a key part in helping NASA maintain this important role.

The NASA STI Program Office is operated by Langley Research Center, the Lead Center for NASA's scientific and technical information. The NASA STI Program Office provides access to the NASA STI Database, the largest collection of aeronautical and space science STI in the world. The Program Office is also NASA's institutional mechanism for disseminating the results of its research and development activities. These results are published by NASA in the NASA STI Report Series, which includes the following report types:

- TECHNICAL PUBLICATION. Reports of completed research or a major significant phase of research that present the results of NASA programs and include extensive data or theoretical analysis. Includes compilations of significant scientific and technical data and information deemed to be of continuing reference value. NASA's counterpart of peer-reviewed formal professional papers but has less stringent limitations on manuscript length and extent of graphic presentations.

- TECHNICAL MEMORANDUM. Scientific and technical findings that are preliminary or of specialized interest, e.g., quick release reports, working papers, and bibliographies that contain minimal annotation. Does not contain extensive analysis.

- CONTRACTOR REPORT. Scientific and technical findings by NASA-sponsored contractors and grantees.

- CONFERENCE PUBLICATION. Collected papers from scientific and technical conferences, symposia, seminars, or other meetings sponsored or cosponsored by NASA.

- SPECIAL PUBLICATION. Scientific, technical, or historical information from NASA programs, projects, and missions, often concerned with subjects having substantial public interest.

- TECHNICAL TRANSLATION. English-language translations of foreign scientific and technical material pertinent to NASA's mission.

Specialized services that complement the STI Program Office's diverse offerings include creating custom thesauri, building customized databases, organizing and publishing research results . . . even providing videos.

For more information about the NASA STI Program Office, see the following:

- Access the NASA STI Program Home Page at ***http://www.sti.nasa.gov***

- E-mail your question via the Internet to help@sti.nasa.gov

- Fax your question to the NASA Access Help Desk at 301–621–0134

- Telephone the NASA Access Help Desk at 301–621–0390

- Write to:
  NASA Access Help Desk
  NASA Center for AeroSpace Information
  7121 Standard Drive
  Hanover, MD 21076

NASA/TM—2004-213066

Detailed Microstructural Characterization of the Disk Alloy ME3

Timothy P. Gabb
Glenn Research Center, Cleveland, Ohio

Anita Garg
University of Toledo, Ohio

David L. Ellis and Kenneth M. O'Connor
Glenn Research Center, Cleveland, Ohio

National Aeronautics and
Space Administration

Glenn Research Center

May 2004

Acknowledgments

The NASA/General Electric/Pratt & Whitney HSR/EPM disk program is acknowledged for producing the disks. The NASA Ultra Efficient Engine Technologies program, Task Manager, Robert Draper, is acknowledged for supporting this work. The authors also wish to acknowledge the many helpful microstructure discussions with David Mourer, Dan Backman, and Jon Groh at General Electric Aircraft Engines; and Paul Reynolds and Rick Montero, Pratt & Whitney Engine Company.

Available from

NASA Center for Aerospace Information
7121 Standard Drive
Hanover, MD 21076

National Technical Information Service
5285 Port Royal Road
Springfield, VA 22100

Available electronically at http://gltrs.grc.nasa.gov

Detailed Microstructural Characterization of the Disk Alloy ME3

Timothy P. Gabb
National Aeronautics and Space Administration
Glenn Research Center
Cleveland, Ohio 44135

Anita Garg*
University of Toledo
Toledo, Ohio 43606

David L. Ellis and Kenneth M. O'Connor
National Aeronautics and Space Administration
Glenn Research Center
Cleveland, Ohio 44135

Abstract

The advanced powder metallurgy disk alloy ME3 was designed using statistical screening and optimization of composition and processing variables in the NASA/General Electric/Pratt & Whitney HSR/EPM disk program to have extended durability for large disks at maximum temperatures of 600 to 700 °C. Scaled-up disks of this alloy were then produced at the conclusion of that program to demonstrate these properties in realistic disk shapes. The objective of the present study was to assess the microstructural characteristics of these ME3 disks at two consistent locations, in order to enable estimation of the variations in microstructure across each disk and across several disks of this advanced alloy. Scaled-up disks processed in the HSR/EPM Compressor/Turbine Disk program had been sectioned, machined into specimens, and tested in tensile, creep, fatigue, and fatigue crack growth tests by NASA Glenn Research Center, in cooperation with General Electric Engine Company and Pratt & Whitney Aircraft Engines. For this study, microstructures of grip sections from tensile specimens in the bore and rim were evaluated from these disks. The major and minor phases were identified and quantified using transmission electron microscopy (TEM). Particular attention was directed to the γ′ precipitates, which along with grain size can predominantly control the mechanical properties of superalloy disks.

Introduction

The advanced powder metallurgy disk alloy ME3 was designed in the NASA/General Electric/ Pratt & Whitney High Speed Research/Enabling Propulsion Materials (HSR/EPM) disk program to have extended durability at 600 to 700 °C in large disks. This was achieved by designing a disk alloy with moderately high γ′ precipitate content and refractory element levels optimized with rapid cooling supersolvus heat treatments to produce balanced monotonic, cyclic, and time-dependent mechanical properties. The resulting baseline alloy with optimized processing, and supersolvus heat treatment has shown extended durability, combined with robust processing and manufacturing characteristics (refs. 1 and 2). It is well known that grain size strongly influences the mechanical properties of disk superalloys (ref. 3). This is clearly established for powder metallurgy (PM) disk superalloys, where grain size and uniformity can be well controlled through careful design of the consolidation, extrusion, forging, and heat treatment processing steps (ref. 4). Grain sizes as small as 5 to 10 μm diameter can be commonly

* NASA Resident Research Associate at Glenn Research Center.

achieved in superalloy disks by using solution heat treatments below the solvus of the γ′ phase, which constrains grain growth. These “subsolvus” heat treatments can produce high tensile strength and fatigue crack initiation resistance. Heat treatments above the γ′ phase solvus (“supersolvus”) dissolve all of the precipitates, allowing grains to grow much larger. Generally speaking, increasing grain size can decrease monotonic strength and fatigue crack initiation resistance, while increasing creep and dwell fatigue crack growth resistances (refs. 5 to 7).

It is also well known that the content and size of strengthening γ′ phase precipitates also influence the mechanical properties of disk superalloys. Three general size ranges of γ′ phase precipitates are usually observed in disk superalloys. Large 1 to 10 μm diameter “primary” γ′ precipitates can be influenced by all thermomechanical processing steps, but are ultimately controlled by the solution heat treatment temperature and time. A subsolvus heat treatment allows some of these precipitates to survive and constrain grain growth. A supersolvus heat treatment temperature can dissolve all of these precipitates. Smaller 0.1 to 1.0 μm “secondary” diameter γ′ precipitates nucleate and begin growing early during quench from the solution heat treatment, generally at temperatures above about 900 °C. Secondary γ′ precipitate size is also influenced by solution heat treatment temperature, but is predominantly set by the cooling rate and path from the solution heat treatment. During the quench from the solution heat treatment temperature, multiple populations of secondary γ′ precipitates can nucleate, grow, and coarsen (ref. 8). Finest “tertiary” γ′ precipitates less than 0.1 μm in diameter subsequently nucleate and begin growing at temperatures below about 900 °C, during the later part of the quench and subsequent stress relief and aging heat treatments. Tertiary γ′ precipitate size is influenced by the cooling path of the quench from solution heat treatment, and also subsequent stress relief and aging heat treatment temperatures and times.

The coarse primary γ′ particles are not reported to provide much strengthening. Increasing content and decreasing size of the secondary γ′ precipitates can strongly increase monotonic strength, fatigue resistance, and creep resistance (refs. 3, and 9 to 11). The effects of tertiary γ′ phase content and size of on mechanical properties are less dramatic, and can be alloy/property dependent.

A detailed characterization of grain sizes, as well as the size distributions and quantities of the multiple possible populations of γ′ precipitates is therefore necessary to quantitatively relate processing paths to the resulting microstructure, and then to relate the microstructure to the resulting mechanical properties. The development of such quantitative relationships is key to improving the processing and mechanical properties of existing disk alloys, and is also essential to reduce risk for introduction of newly developed disk alloys such as ME3.

The objective of this study was to assess the detailed microstructural characteristics of the scaled-up disk alloy ME3. Scaled-up disks processed in the HSR/EPM Compressor/Turbine Disk program had been sectioned, machined into specimens, and tested in tensile, creep, fatigue, and fatigue crack growth tests by NASA Glenn Research Center, in cooperation with General Electric Engine Company and Pratt & Whitney Aircraft Engines. Microstructures of grip sections from a tensile specimen in the bore and a notched tensile specimen in the rim were evaluated from these disks. The major and minor phases were identified and quantified. Particular attention was directed to the measurement of grain size and γ′ precipitate size, both of which control the mechanical properties in disk superalloys.

Materials and Procedure

Eight scaled-up baseline ME3 disks were either subsolvus or supersolvus solution heat treated. Disk identifications and processing steps are listed in table 1. Each disk had a maximum diameter of near 60 cm, a maximum thickness in the bore of near 10 cm, and a maximum thickness in the rim of near 5 cm. Quench rate and stress relief heat treatment time were varied among these disks. The disks were quenched using fan air cooling followed by oil quenching, with varied time sequence intervals. One of two subsequent stress relief heat treatment times was applied, followed by a fixed final aging heat

treatment step. The grip sections of a tensile specimen (T1) in the slow cooling bore location and a notched tensile specimen (NT4) from a faster cooling rim location were evaluated from each disk, after being tensile tested.

Pins of 3 mm diameter were extracted by electrodischarge machining parallel to the loading axis from the grip of the selected tensile specimens. A low speed abrasive saw was used to cut slices about 0.5 mm thick from each pin. The slices were mechanically polished down to about 140 to 150 μm thickness, then electrochemically thinned using a solution of 10 percent Perchloric acid, 90 percent Methanol mixture cooled to –25 to –30 °C. Grain sizes were also later determined on metallographically prepared sections of the same specimen grip sections, according to ASTM E–112 linear intercept procedures, using circular grid overlays on 5 randomly selected images for each specimen.

γ′ precipitates were consistently imaged using <010> dark field reflections near the <001> zone axis. This was performed on grains selected with a <001> zone axis oriented less than 30° from the beam axis, to avoid excessive foil tilting. At least 4 foils were surveyed from each specimen. Image analyses of the γ′ precipitates were performed using SigmaScan™ software. Area fractions of primary and secondary γ′ precipitates were measured by point counting, from metallographic sections and very thin regions of the TEM foil, respectively. Area fractions of tertiary γ′ were estimated as the difference between the total γ′ phase content and any measured primary/secondary phase contents. A minimum of 100 secondary and 100 tertiary γ′ precipitates were measured for size quantification in each specimen. Major and minor axis lengths and area were directly measured by the software. Several shape parameters including aspect ratio, feret diameter, compactness, and shape factor were then calculated as illustrated in figure 1. Maximum and minimum values were tabulated, along with averages and standard deviations calculated assuming a single, normal distribution in each case. Frequency distributions of feret diameter were further analyzed using Peakfit™ software, and the associated histograms and fitted curves were prepared, with the peak values indicated for each curve in the figures.

Results and Discussion

General Microstructure

The grain sizes of specimens from each disk selected for detailed microstructural evaluations are listed in table 1. Mean grain sizes of supersolvus heat treated specimens were comparable at ASTM 6.5 to 7.6 (23 to 34 μm) and standard deviations in ASTM number of 0.1 to 0.4. Subsolvus heat treated specimens had comparable ASTM 11.9 to 12.1 (4.9 to 5.2 μm) grain size and standard deviations in ASTM number of 0.1 to 0.3. As-large-as (ALA) grain sizes of supersolvus heat treated specimens were comparable at ASTM 2.3 to 4, while subsolvus heat treated specimens had ASTM 7.3 to 8.5 ALA grain sizes. Typical microstructures of specimens etched in Kallings reagent are shown in figures 2 to 4. Although their grain sizes were roughly the same, bore specimens of supersolvus disks consistently had slightly coarser grain sizes and more irregular, serrated grain boundaries than rim specimens, as shown in figure 3.

The total γ′ phase content in ME3 was measured at an area fraction of 0.517 ± 0.008. This was based on point counting measurements from a sectioned specimen given a very slow quench time of 3 weeks from the supersolvus heat treatment temperature to 870 °C, to allow all γ′ phase to precipitate and grow at near equilibrium conditions. The resulting γ′ phase precipitates in this specimen were very large at 1 to 3 μm diameter. In the supersolvus heat treated disks, all observed γ′ phase was in the form of “secondary” precipitates of 0.1 to 0.6 μm diameter taking up an area fraction of 0.49 to 0.52 and “tertiary” precipitates

of 0.01 to 0.04 μm diameter taking up an area fraction of 0.001 to 0.03. In the subsolvus heat treated disks, un-dissolved "primary" γ′ phase took up an area fraction of 0.152 ± 0.015, in the form of large particles 0.8 to 5 μm in diameter.

Minor phases were identified by surveying the general microstructure of multiple foils at low magnifications, as shown in figures 5 to 11. Identified phases were then evaluated at high magnifications using selected area electron diffraction patterns and qualitative energy dispersive x-ray analyses. The observed minor phases were similar in supersolvus and subsolvus heat treated disks. Results for the supersolvus disks are summarized in table 2, with minor phases compared separately for within grains and at grain boundaries. MC carbides of 150 to 700 nm diameter were the predominant minor phase observed within grains, accounting for 88 percent by number of the minor phases typically observed. Their qualitative phase chemistry was (Ti,Ta,Nb,Mo)C. Approximately 5 percent of the secondary particles were M_3B_2 borides ranging from 400 to 1000 nm in diameter. Their composition was determined to be $(Mo,Cr,W)_3B_2$. About 5 percent of smaller ZrO_2 oxides and 2 percent of Al_2O_3 oxides were also observed with grains. At the grain boundaries, $M_{23}C_6$ carbides predominated, having compositions of $(Cr,Mo,W)_{23}C_6$. A small number of larger MC carbides also resided there, and very sparse quantities of $(Mo,Cr,W)_3B_2$ borides, Al_2O_3 oxides, and ZrO_2 oxides at the grain boundaries.

Detailed γ′ Evaluations

Supersolvus heat treated disks.—Typical secondary and tertiary γ′ microstructures observed within grains are compared for the bore and rim specimens of each supersolvus heat treated disk in figure 12. Histograms of γ′ size-frequency measurements are likewise compared in figures 13 and 14. Sizes, shape parameters, and area fractions are summarized in tables 3 to 6. Visual inspection suggests the bore specimens had larger sizes and possibly lower area fractions of secondary γ′ than the rim specimens. The larger secondary γ′ precipitates in bore specimens often had multiple lobes extending out diagonally from the {001} cube plane faces. The observation and description of such γ′ precipitate growth has previously been described (ref. 12). Bore specimens also appeared to have a wider variation in secondary γ′ sizes than in the rim specimens. This sometimes appeared due to the sectioning of the lobed tips for the larger γ′ precipitates. However, smaller isolated secondary γ′ precipitates appeared to also be present in the microstructure. Rim specimens had a more uniform population of rounded cuboid γ′ precipitates, which appeared smaller in size and had only very minor lobe growth at the cube corners. The tertiary γ′ precipitates appeared similar in size and shape for all supersolvus heat treated specimens.

The results of quantitative image analyses of the secondary and tertiary γ′ within the grains of supersolvus disk specimens are summarized in tables 3 to 6 and table 11. Feret diameters, which are insensitive to minor precipitate shape differences, were used in these comparisons. The measured averages of secondary γ′ major axis, minor axis, and feret diameter of the bore specimens varied with disk quench rate. The slower quenched bore specimens from S100 and S101 disks had higher mean sizes than the faster quenched bore specimens of W110 and H111 disks. The mean secondary γ′ precipitate sizes did not strongly vary with the disk quench rate in the rim specimens. Overall, mean secondary γ′ feret diameter was inversely correlated with relative cooling rate, figure 15. However, this is an overly simplified conclusion, as it will be shown that these specimens had bimodal secondary γ′ size distributions. The bore specimens of all four supersolvus disks had higher compactness and lower shape factors than the rim specimens, consistent with the presence of pronounced multi-lobed particles in the bores. Compactness and shape factor values for the rim specimens were between those expected for round and cuboidal shaped secondary γ′. No clear trend was observed between relative stress relief time and secondary γ′ size, figure 15. Stepwise multiple linear regression of size versus relative cooling rate, stress relief time, and their interaction term also confirmed that only the cooling rate had a statistically significant effect.

Histograms of feret diameter versus frequency are compared for secondary γ′ in figure 13 and tertiary γ′ in figure 14. A wide variation of secondary γ′ sizes in bore specimens is clearly evident in the histograms. Two size populations of secondary γ′ could be separated for each of the bore specimens, with peak values differing by about a factor of 2 between the smaller sized "S1" population and the larger sized "S2" population. As reflected in the 2X factor, the S1 population was made up in part by the random sectioning of the large lobed particles through the outer diagonal lobes. These lobes did appear to be nearly half the size of the main particle. However, the S1 population was also made up in part by isolated, small secondary γ′ precipitates. In comparing the bore specimens of the slower quenched, S100 and S101, disks with those of the faster quenched, W110 and H111, disks, it is apparent the S2 population predominated in the slower quenched disk cases, while the S1 population predominated in the faster quenched disk cases. This trend is consistent with the results for the even faster cooled rim specimens from each disk. Here, the S2 population was not observed at all, and the S1 population clearly predominated. In the rim specimens, the size histograms for all four supersolvus heat treated disks were comparable. When segregated S1 and S2 secondary γ′ sizes, as measured by the center of the fitted peaks, are compared versus heat treatment, it can be seen these sizes did not strongly vary with quench rate or relative stress relief time, figure 16 and table 11. Stepwise multiple linear regression also could find no statistically significant dependencies. So the cooling rate dependence observed for overall mean sizes of figure 15 is principally due to the relative quantities of S1 and S2 precipitates.

Mean sizes and histograms of feret diameter versus frequency for the tertiary γ′ did not strongly vary with cooling rate between the supersolvus disks. Only a weak correlation ($R^2 = 0.41$) of decreasing size as a function of increasing cooling rate was identified. Rather, the bore specimens of all disks had a common larger size than that of the rim specimens. This could be because the instantaneous cooling rates in the latter intervals of the quench process were similar for the bores of all disks, and similar for the rims of all disks. The subsequent stress relief and aging heat treatments could then have coarsened the tertiary γ′ to similar, near equilibrium sizes. However, it should be noted that the smallest tertiary γ′ size was measured in the rim of the faster quenched disk given the short stress relief heat treatment, W110.

The microstructures at the grain boundaries of these specimens are compared in figures 17 to 20. Optical images of etched metallographic sections showed the bore specimens consistently have more undulated, serrated grain boundaries than the rim specimens, figure 3. TEM imaging of grain boundaries in thin foils indicated the serrations were produced by enlarged secondary γ′ which protruded into the grain boundary. This enlargement was greater for the bore specimens. This response has been observed elsewhere (ref. 13), and could be attributed to enhanced diffusion of γ′ forming elements along the grain boundary during the long time excursions near the solvus of the slower cooling bore specimens.

Subsolvus heat treated disks.—The typical secondary and tertiary γ′ microstructures within the grains of rim specimens from subsolvus heat treated disks are shown in figure 21. Visual inspection suggests finer secondary γ′ size in the rims of faster quenched disks S010 and W011 than for slower quenched, W000 and S001, disks, with similar area fractions. Measured sizes, area fractions, and shape parameters are compared in tables 7 to 11, and histograms of size versus frequency are shown in figures 22 and 23. Feret diameter of secondary γ′ could be considered normally distributed for all four cases, and only a single population was obvious for each specimen, so the trends observed from averaged values correspond well to the size histograms. Averaged secondary γ′ sizes were smaller for the faster quenched disks, with similar standard deviations, figure 16. These sizes did not clearly vary with relative stress relief time. It should be noted that more variations in secondary γ′ could be possible in the bores of subsolvus heat treated disks, not evaluated in this study.

Tertiary γ′ size did not clearly vary with quench rate or stress relief time in these subsolvus heat treated rim specimens. However, the histograms of feret diameter were skewed towards large size for the longer relative stress relief time, suggesting additional growth of some precipitates with longer time.

The mean sizes of secondary γ′ for subsolvus disk rim specimens were similar to those of the S1 precipitates in supersolvus disks, figure 16 and table 11. The higher relative cooling rates encountered in the fastest quenched subsolvus disks S010 and W011 produced slightly smaller sizes. Tertiary γ′ sizes were comparable for subsolvus and supersolvus disks.

The microstructures at the grain boundaries of these specimens are compared in figure 24. TEM imaging of grain boundaries in thin foils indicated relatively flat, un-serrated grain boundaries. The primary γ′ particles often pinned triple point intersections of grain boundaries, and were encircled by a zone having only tertiary γ′ precipitates.

Summary and Conclusions

The microstructures of specimens from the bores and rims of supersolvus and subsolvus heat treated ME3 disks were evaluated using optical and transmission electron microscopy. The findings can be summarized as follows:

1. Mean and ALA grain sizes of bore and rim specimens from supersolvus heat treated disks were comparable and well-controlled, with mean ASTM grain sizes of 6.5 to 7.5 and ALA grain sizes of 2.3 to 4.0.
2. Mean and ALA grain sizes of rim specimens from subsolvus heat treated disks were also comparable and well-controlled, with mean grain sizes of 11.9 to 12.1 and ALA grain sizes of 7.3 to 8.5.
3. Secondary γ′ precipitates in supersolvus heat treated disks could be separated into two populations of smaller, more regular shaped S1 precipitates and larger, more distorted S2 precipitates. The size of the S1 and S2 precipitates did not clearly vary with cooling rate or stress relief time. However, the relative proportion of smaller S1 precipitates increased with cooling rate.
4. Tertiary γ′ precipitate size did not clearly vary between supersolvus heat treated disks, but was dependent on disk location. Precipitate sizes in bore specimens were larger than those for rim specimens. No significant size dependence with stress relief time was evident.
5. Secondary γ′ precipitate size was found to moderately decrease with increasing cooling rate for specimens from the rims of subsolvus solution heat treated disks.

It can be concluded from this work that:

1. The grain size variations in subsolvus as well as supersolvus heat treated ME3 can be controlled well with respect to other powder metallurgy disk alloys, and better than typical cast and wrought disk alloys.
2. Secondary γ′ precipitates in supersolvus heat treated superalloy disks can have bimodal size distributions, probably due to different successive bursts of nucleation. Quantification of the precipitates in these cases can be refined by size frequency analysis and peak fitting.
3. The effects of varying quench rate on secondary γ′ precipitate size can be more complicated than monotonic size changes. Increasing quench rates apparently encouraged a higher frequency of nucleation for S1 precipitates, and a lower frequency of nucleation for S2 precipitates. A full understanding of this relationship would require application of γ′ precipitate nucleation models such as in reference 8.
4. The effects of varying quench rate on tertiary γ′ precipitate size appeared related to relative disk location, and associated quench rate during the latter stages of the quench. Slower cooling bore specimens had larger tertiary γ′ precipitate size. The effects of varying stress relief time were inconsequential over the range of these heat treatments.
5. Overall, it can be concluded that such a detailed quantification of microstructure can be useful for generation of processing, microstructure, and mechanical property relationships and models.

References

1. T.P. Gabb, J. Gayda, and J. Telesman, "Development of Advanced Powder Metallurgy Disk Alloys in NASA-Industry Programs," Aeromat 2001, Long Beach, CA, June 14, 2001.
2. T.P. Gabb, J. Gayda, J. Telesman, P.T. Kantzos, and W.A. Konkel, "Realistic Subscale Evaluations of the Mechanical Properties of Advanced Disk Superalloys," NASA/TM—2003-212086.
3. C.T. Sims, N.S. Stoloff, and W.C. Hagel, Superalloys II, John Wiley & Sons, New York, NY, pp. 66–77.
4. D.M. Chang, D.D. Krueger, and R.A. Sprague, Superalloys 1984, eds. M. Gell, C.S. Kortovich, R.H. Bricknell, W.B. Kent, and J.F. Radavich, TMS, Warrendale, PA, 1984, pp. 247–273.
5. J.J. Schirra and S.H. Goetschius, in Superalloys 1992, eds. S.D. Antolovich, R.W. Stusrud, R.A. MacKay, D.L. Anton, T. Khan, R.D. Kissinger, and D.L. Klarstrom, TMS, Warrendale, PA, 1992, pp. 437–446.
6. R.V. Miner, J. Gayda, and R.D. Maier, Met. Trans. A, V. 13A, 1982, pp. 1755–1765.
7. J. Gayda, R.V. Miner, and T.P. Gabb, Superalloys 1984, eds. M. Gell, C.S. Kortovich, R.H. Bricknell, W.B. Kent, and J.F. Radavich, TMS, Warrendale, PA, 1984, pp. 733–742.
8. T.P. Gabb, D.G. Backman, D.Y. Wei, D.P. Mourer, D.U. Furrer, A. Garg, and D.L. Ellis, Superalloys 2000, eds. T.M. Pollock, R.D. Kissinger, R.R. Bowman, K.A. Green, M. McLean, S.L. Olson, and J.J. Schirra, TMS, Warrendale, PA, 2000, pp. 405–414.
9. K. Harris, G.L. Erickson, and R.E. Schwer, Superalloys 1984, eds. M. Gell, C.S. Kortovich, R.H. Bricknell, W.B. Kent, and J.F. Radavich, TMS, Warrendale, PA, 1984, pp. 221–230.
10. J. Groh, Superalloys 2000, eds. T.M. Pollock, R.D. Kissinger, R.R. Bowman, K.A. Green, M. McLean, S.L. Olson, and J.J. Schirra, TMS, Warrendale, PA, 2000, pp. 621–626.
11. R.A. Ricks, A.J. Porter, and R.C. Ecob, Acta Met., V. 31, 1983, pp. 43–53.
12. H. Loyer Danflou, M. Marty, and A. Walder, Superalloys 1992, eds. S.D. Antolovich et al., TMS, Warrendale, PA, 1992, pp. 63–72.
13. H. Loyer Danflou, M. Macia, T.H. Sanders, and T. Khan, Superalloys 1996, eds. R.D. Kissinger, K.J. Deye, K.L. Anton, A.D. Cetel, M.V. Nathal, T.M. Pollock, and D.A. Woodford, TMS, Warrendale, PA, 1996, pp. 119–127.

Table 1.—Disk and specimen identifications, processing, and grain sizes

Disk ID	Solution Heat Treat	Relative Quench Rate	Relative Stress Relief Time	Specimen	Location	Mean Grain Size-µm	Mean Grain Size-ASTM No.	Stan. Dev. Grain Size-ASTM No.	As-Large-As Grain Size-ASTM No.
S100	Supersolvus	1.00	1.00	T1	Bore	25	7.4	0.1	4
		1.52	1.20	NT4	Rim	28.7	7	0.2	3.3
S101	Supersolvus	1.17	2.06	T1	Bore	24.1	7.5	0.1	4
		1.52	2.11	NT4	Rim	28.2	7	0.4	3
W110	Supersolvus	1.33	1.00	T1	Bore	29.5	6.9	0.1	3.5
		2.05	1.20	NT4	Rim	34.2	6.5	0.4	2.3
H111	Supersolvus	1.33	1.91	T1	Bore	23	7.6	0.2	3.5
		2.05	2.11	NT4	Rim	30.6	6.8	0.2	3.3
W000	Subsolvus	1.86	1.20	NT4	Rim	4.9	12.1	0.3	7.3
S001	Subsolvus	1.86	2.11	NT4	Rim	5	12	0.2	8
S010	Subsolvus	3.38	1.20	NT4	Rim	5.2	11.9	0.1	8.5
W011	Subsolvus	3.38	2.11	NT4	Rim	4.9	12	0.1	8

Table 2.—Minor phases identified in supersolvus disks: percent of minor phases and size ranges

	S100				S101				W110				H111			
		Bore-T1		Rim-NT4		Bore-T1		Rim-NT4		Bore-T1		Rim-NT4		Bore-T1		Rim-NT4
	%	Size Range	%	Size Range	%	Size Range	%	Size Range	%	Size Range	%	Size Range	%	Size Range	%	Size Range
MINOR PHASES IN MATRIX																
(Ti,Ta,Nb,Mo)C	88	200-650	88	200-600	88	150-600	88	200-650	88	200-600	88	150-700	88	200-600	88	150-650
$(Mo,Cr,W)_3B_2$	5	500-1000	5	400-600	5	400-800	5	500	5	500-1000	5	500-700	5	500-800	5	500-700
Al_2O_3	2	<150	2	<150	2	<150	2	<100	2	<150	2	<150	2	<150	2	<150
ZrO_2	5	<200	5	<250	5	<250	5	<250	5	<200	5	<250	5	<200	5	<200
MINOR PHASES AT GRAIN BOUNDARIES																
$(Cr,Mo,W)_{23}C_6$	90	200	90	<120	90	150	90	<150	90	200	90	<150	90	200	90	<150
(Ti,Ta,Nb,Mo)C	5	400-600	5	200-450	5	500-6500	5	400-550	5	400-600	5	300-600	5	450-600	5	450-600
$(Mo,Cr,W)_3B_2$	S		S		S		S		S	<600	S		S	<500	S	
Al_2O_3	S		S		S		S		S		S	<150	S		S	
ZrO_2	S		S	<200	S	<250	S	<200	S	<200	S	<200	S	<200	S	
Notes:	1) Dimensions in nanometers (10^{-9} m)								2) S=Sparsely scattered minor phases							

Table 3.—Size measurements of γ′ within grains of specimens from bore (T1) and rim (NT4) of disk S100

(a) S100-bore

Type of γ'	Number	Area Fraction		Major Axis (nm)	Minor Axis (nm)	Feret Diameter (nm)	Aspect Ratio	Compactness	Shape Factor
Secondary	311	0.49	Average	408.51	319.68	327.18	0.78	22.54	0.60
			σ	122.10	109.48	91.68	0.12	7.40	0.15
			Minimum	112.68	94.84	96.98	0.41	14.30	0.16
			Maximum	767.68	642.69	590.76	0.99	80.62	0.88
Tertiary	106	0.03	Average	30.02	24.26	27.69	0.82	13.95	0.91
			σ	8.10	6.29	6.54	0.10	1.01	0.06
			Minimum	12.66	10.23	12.53	0.49	11.95	0.74
			Maximum	56.65	40.02	44.72	1.00	17.06	1.05

(b) S100-rim

Type of γ'	Number	Area Fraction		Major Axis (nm)	Minor Axis (nm)	Feret Diameter (nm)	Aspect Ratio	Compactness	Shape Factor
Secondary	388	0.52	Average	230.08	182.25	194.16	0.79	16.37	0.78
			σ	51.39	51.82	43.12	0.12	1.77	0.07
			Minimum	73.81	60.79	63.48	0.40	14.11	0.51
			Maximum	396.12	362.61	313.38	1.00	24.85	0.89
Tertiary	622	<0.01	Average	26.27	22.36	25.08	0.86	13.75	0.92
			σ	7.57	6.36	6.43	0.09	1.07	0.07
			Minimum	8.95	5.55	9.70	0.53	10.89	0.65
			Maximum	55.11	46.69	46.88	1.00	19.23	1.15

Table 4.—Size measurements of γ′ within grains of specimens from bore (T1) and rim (NT4) of disk S101

(a) S101-bore

Type of γ'	Number	Area Fraction		Major Axis (nm)	Minor Axis (nm)	Feret Diameter (nm)	Aspect Ratio	Compactness	Shape Factor
Secondary	139	0.51	Average	385.67	311.66	316.22	0.81	20.12	0.65
			σ	116.06	104.40	86.47	0.11	4.67	0.13
			Minimum	136.58	102.78	126.68	0.54	14.22	0.29
			Maximum	697.09	643.27	529.51	0.99	42.90	0.88
Tertiary	241	0.01	Average	37.92	31.50	35.01	0.84	14.24	0.89
			σ	12.03	9.73	10.08	0.09	1.16	0.07
			Minimum	10.32	7.92	10.57	0.54	12.14	0.64
			Maximum	81.50	65.51	66.60	1.00	19.75	1.04

(b) S101-rim

Type of γ'	Number	Area Fraction		Major Axis (nm)	Minor Axis (nm)	Feret Diameter (nm)	Aspect Ratio	Compactness	Shape Factor
Secondary	559	0.52	Average	229.26	177.41	193.22	0.77	15.89	0.80
			σ	54.77	50.52	44.64	0.12	1.40	0.06
			Minimum	102.75	64.40	86.22	0.39	13.67	0.54
			Maximum	440.85	391.76	374.27	1.00	23.23	0.92
Tertiary	411	<0.01	Average	30.04	24.16	27.71	0.81	14.21	0.89
			σ	9.09	7.30	7.56	0.11	1.24	0.07
			Minimum	11.10	0.00	11.88	0.00	11.99	0.57
			Maximum	68.83	52.36	59.54	1.00	21.89	1.05

Table 5.—Size measurements of γ′ within grains of specimens from bore (T1) and rim (NT4) of disk W110

(a) W110-bore

Type of γ'	Number	Area Fraction		Major Axis (nm)	Minor Axis (nm)	Feret Diameter (nm)	Aspect Ratio	Compactness	Shape Factor
Secondary	246	0.51	Average	317.90	235.04	248.20	0.75	25.87	0.59
			σ	166.10	125.55	117.89	0.13	14.70	0.20
			Minimum	81.99	58.44	66.54	0.35	14.06	0.13
			Maximum	876.28	617.14	598.56	0.98	99.05	0.89
Tertiary	656	0.01	Average	42.82	34.81	38.90	0.82	14.43	0.88
			σ	19.32	15.46	16.38	0.09	1.26	0.07
			Minimum	12.52	9.03	12.63	0.51	11.53	0.52
			Maximum	144.68	120.83	131.03	1.00	24.21	1.09

(b) W110-rim

Type of γ'	Number	Area Fraction		Major Axis (nm)	Minor Axis (nm)	Feret Diameter (nm)	Aspect Ratio	Compactness	Shape Factor
Secondary	678	0.51	Average	221.56	177.11	188.81	0.80	16.09	0.79
			σ	49.04	49.43	40.78	0.11	1.73	0.07
			Minimum	60.23	48.35	54.80	0.43	13.84	0.36
			Maximum	526.17	513.12	429.74	1.00	34.76	0.91
Tertiary	653	0.01	Average	19.20	16.10	18.14	0.84	14.07	0.90
			σ	5.72	4.99	4.91	0.09	1.41	0.08
			Minimum	6.67	4.14	6.60	0.49	11.32	0.58
			Maximum	39.02	32.93	33.79	1.00	21.70	1.11

Table 6.—Size measurements of γ′ within grains of specimens from bore (T1) and rim (NT4) of disk H111

(a) H111-bore

Type of γ'	Number	Area Fraction		Major Axis (nm)	Minor Axis (nm)	Feret Diameter (nm)	Aspect Ratio	Compactness	Shape Factor
Secondary	180	0.51	Average	299.94	226.70	239.91	0.74	23.20	0.61
			σ	147.15	126.05	112.45	0.13	10.18	0.17
			Minimum	81.73	61.92	72.34	0.30	14.02	0.14
			Maximum	839.87	777.02	668.68	0.95	92.52	0.90
Tertiary	763	0.01	Average	43.22	34.92	38.93	0.81	15.34	0.84
			σ	20.66	16.74	17.71	0.10	2.61	0.10
			Minimum	11.19	5.60	10.94	0.45	11.66	0.29
			Maximum	172.71	122.45	137.56	1.00	42.96	1.08

(b) H111-rim

Type of γ'	Number	Area Fraction		Major Axis (nm)	Minor Axis (nm)	Feret Diameter (nm)	Aspect Ratio	Compactness	Shape Factor
Secondary	951	0.52	Average	226.98	179.72	193.80	0.79	15.59	0.81
			σ	49.69	47.69	40.25	0.11	1.67	0.07
			Minimum	95.25	57.15	83.21	0.36	13.08	0.33
			Maximum	613.57	577.17	507.32	1.00	37.65	0.96
Tertiary	825	<0.01	Average	26.71	22.74	25.52	0.86	13.79	0.92
			σ	7.21	5.80	6.05	0.08	1.21	0.07
			Minimum	7.82	5.53	8.82	0.49	11.66	0.43
			Maximum	72.69	40.91	49.73	1.00	28.95	1.08

Table 7.—Size measurements of γ′ within grains of specimens from rim (NT4) of disk W000

Type of γ'	Number	Area Fraction		Major Axis (nm)	Minor Axis (nm)	Feret Diameter (nm)	Aspect Ratio	Compactness	Shape Factor
Secondary	364	0.43	Average	173.43	136.36	148.66	0.79	16.02	0.79
			σ	37.30	35.07	31.40	0.10	1.83	0.07
			Minimum	71.94	49.88	57.73	0.41	13.90	0.48
			Maximum	289.47	252.82	243.71	1.00	26.16	0.90
Tertiary	308	<0.01	Average	24.17	19.91	22.81	0.83	14.01	0.91
			σ	6.72	5.83	5.76	0.11	1.44	0.09
			Minimum	5.60	0.00	7.47	0.00	11.36	0.63
			Maximum	48.15	35.84	40.14	1.00	19.87	1.11

Table 8.—Size measurements of γ′ within grains of specimens from rim (NT4) of disk S001

Type of γ'	Number	Area Fraction		Major Axis (nm)	Minor Axis (nm)	Feret Diameter (nm)	Aspect Ratio	Compactness	Shape Factor
Secondary	594	0.44	Average	188.23	148.60	162.09	0.79	16.14	0.79
			σ	46.67	42.65	39.98	0.11	1.59	0.07
			Minimum	76.42	55.13	68.32	0.40	13.89	0.42
			Maximum	343.08	294.60	285.57	1.00	29.80	0.91
Tertiary	379	<0.01	Average	28.62	23.59	26.59	0.83	14.26	0.89
			σ	9.42	7.86	7.98	0.10	1.60	0.09
			Minimum	9.03	0.00	10.18	0.00	10.89	0.51
			Maximum	54.90	51.36	50.84	1.00	24.65	1.15

Table 9.—Size measurements of γ′ within grains of specimens from rim (NT4) of disk S010

Type of γ'	Number	Area Fraction		Major Axis (nm)	Minor Axis (nm)	Feret Diameter (nm)	Aspect Ratio	Compactness	Shape Factor
Secondary	254	0.39	Average	154.40	125.47	134.64	0.81	16.30	0.78
			σ	37.37	34.97	32.05	0.10	1.58	0.07
			Minimum	78.56	61.11	69.47	0.50	14.05	0.52
			Maximum	303.83	259.71	251.02	0.99	24.27	0.89
Tertiary	377	<0.01	Average	32.26	26.66	29.37	0.83	15.21	0.84
			σ	11.11	9.49	9.58	0.10	1.93	0.09
			Minimum	10.62	7.08	10.18	0.45	11.49	0.49
			Maximum	70.53	65.27	66.60	1.00	25.47	1.09

Table 10.—Size measurements of γ′ within grains of specimens from rim (NT4) of disk W011

Type of γ'	Number	Area Fraction		Major Axis (nm)	Minor Axis (nm)	Feret Diameter (nm)	Aspect Ratio	Compactness	Shape Factor
Secondary	257	0.39	Average	144.78	118.14	126.37	0.82	15.97	0.80
			σ	42.45	35.66	34.29	0.10	2.42	0.09
			Minimum	52.25	45.93	48.85	0.48	13.79	0.41
			Maximum	331.71	248.73	263.33	0.99	31.04	0.91
Tertiary	217	<0.01	Average	30.91	25.72	28.95	0.84	14.01	0.90
			σ	10.80	8.80	9.20	0.09	1.16	0.07
			Minimum	9.03	5.60	8.93	0.55	11.95	0.55
			Maximum	79.55	61.07	65.94	1.00	22.73	1.05

Table 11.—Summary of comparative size measurements for γ′ precipitates within grains of all specimens

Disk ID	Specimen	Location	Solution Heat Treat	Relative Quench Rate	Relative Stress Relief Time	Mean Secondary γ ' Feret Dia.-nm	Large (S2) Sec. γ ' Hist. Peak-nm	Small (S1) Sec. γ ' Hist. Peak-nm	Mean Tertiary γ ' Feret Dia.-nm	Tertiary γ ' Hist. Peak-nm
S100	T1	Bore	Supersolvus	1.00	1.00	327	368	176	27.69	29
	NT4	Rim		1.52	1.20	194		204	25.08	27
S101	T1	Bore	Supersolvus	1.17	2.06	316	362	214	35.01	33
	NT4	Rim		1.52	2.11	193		201	27.71	28
W110	T1	Bore	Supersolvus	1.33	1.00	248	420	184	38.9	33
	NT4	Rim		2.05	1.20	189		199	18.14	20
H111	T1	Bore	Supersolvus	1.33	1.91	240	412	168	38.93	32
	NT4	Rim		2.05	2.11	194		206	25.52	27
W000	NT4	Rim	Subsolvus	1.86	1.20	149		161	22.81	25
S001	NT4	Rim	Subsolvus	1.86	2.11	162		171	26.59	26
S010	NT4	Rim	Subsolvus	3.38	1.20	135		143	29.37	30
W011	NT4	Rim	Subsolvus	3.38	2.11	126		135	28.95	27

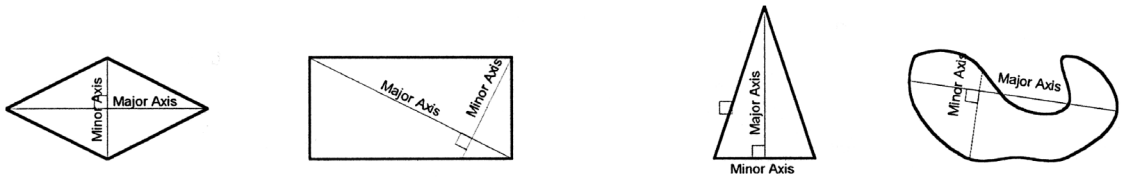

$$\text{Aspect Ratio} = \frac{\text{Minor Axis Length}}{\text{Major Axis Length}}$$ =1 for circle, square, infinite for line

$$\text{Compactness} = \frac{\text{Perimeter}^2}{\text{Area}}$$ $=4\pi$ (12.57) for circle, infinite for line

$$\text{Shape Factor} = \frac{4\pi\,\text{Area}}{\text{Perimeter}^2}$$ =1 for circle, 0.61 for equilateral triangle, 0.79 for square, 0.86 for pentagon

$$\text{Feret Diameter} = \sqrt{\frac{4\,\text{Area}}{\pi}}$$ = diameter of circle with equal area

Figure 1.—Shape parameters calculated in quantification of γ' precipitates.

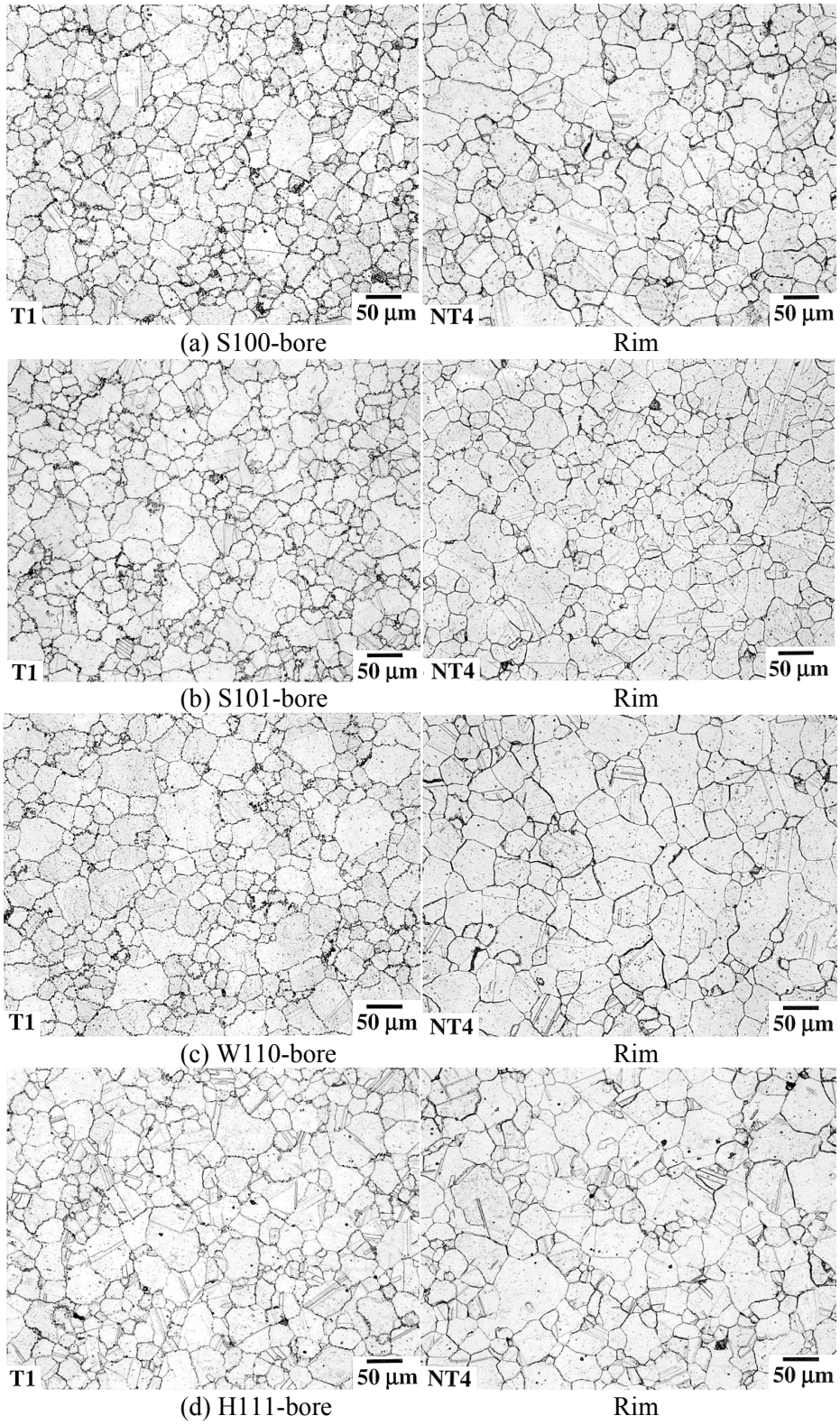

Figure 2.—Grain microstructures of bore (T1) and rim (NT4) specimens from supersolvus heat treated disks: (a) S100, (b) S101, (c) W110, (d) H111.

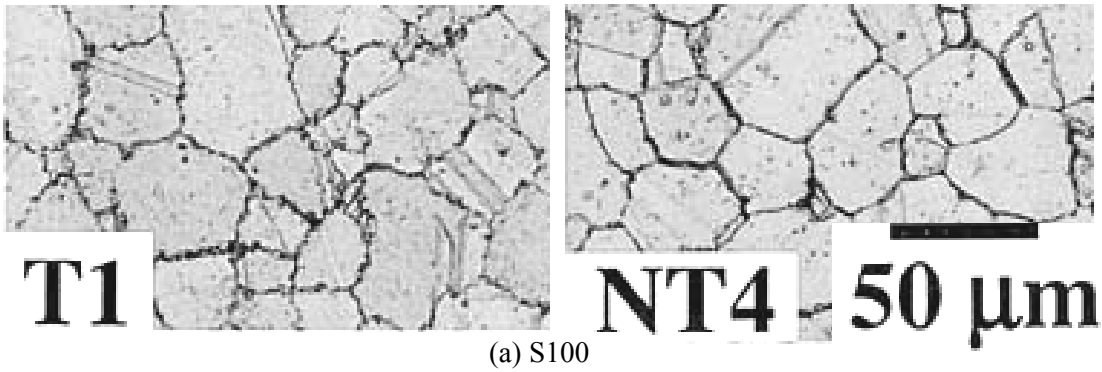

(a) S100

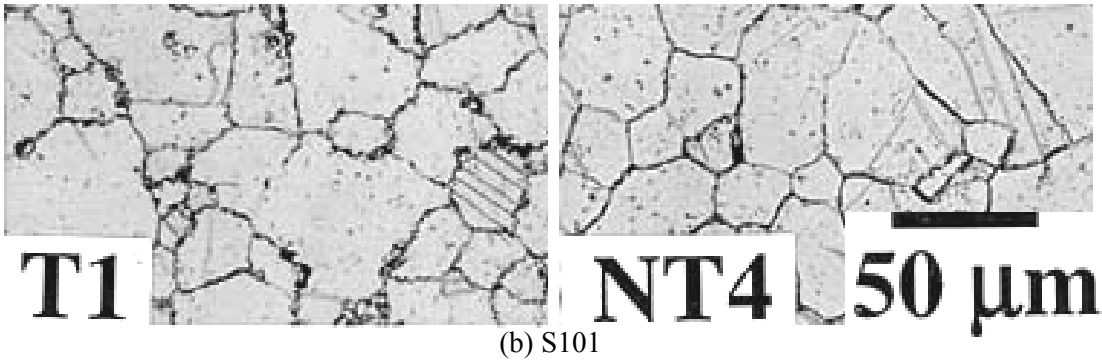

(b) S101

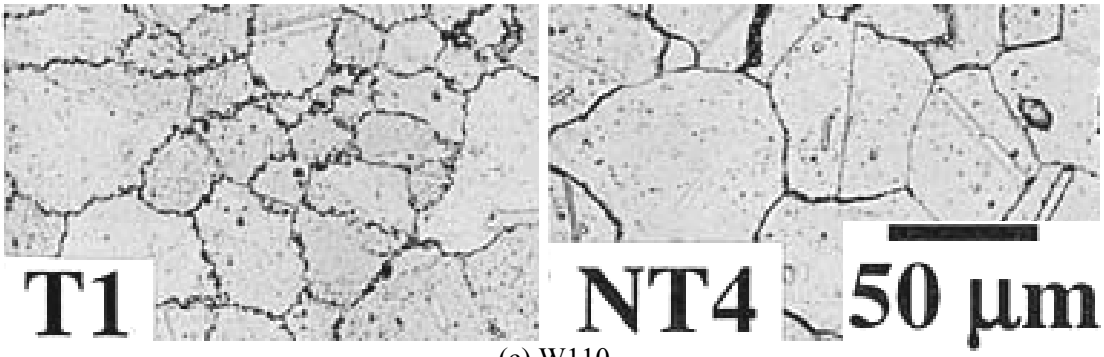

(c) W110

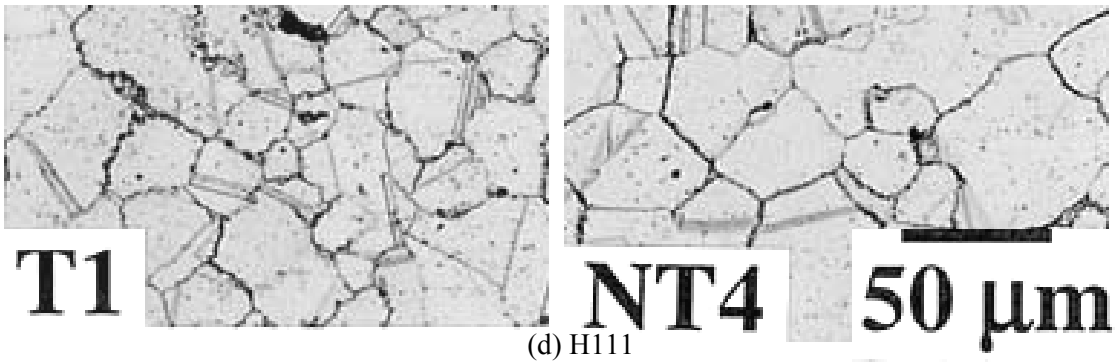

(d) H111

Figure 3.—Grain boundary serrations of disks. (a) S100, (b) S101, (c) W110, (d) H111.

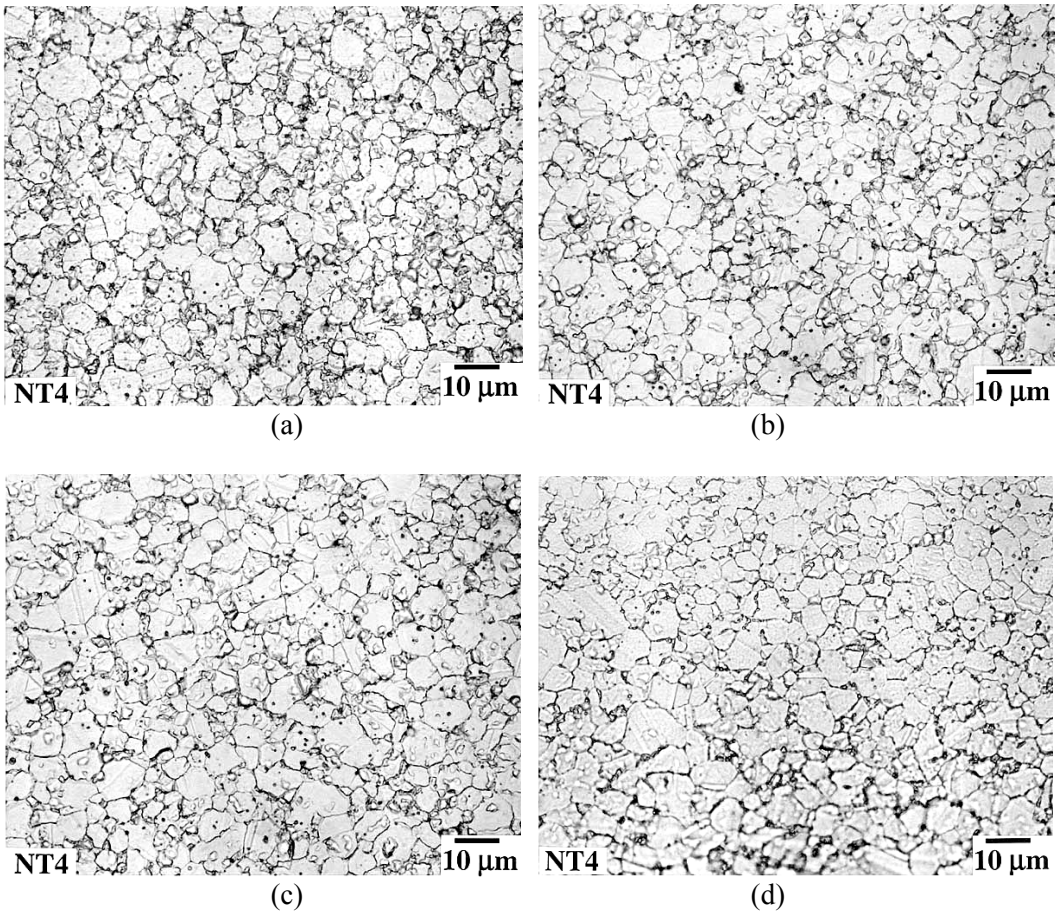

Figure 4.—Grain microstructures of rim (NT4) specimens from subsolvus heat treated disks. (a) W000, (b) S001, (c) S010, (d) W011.

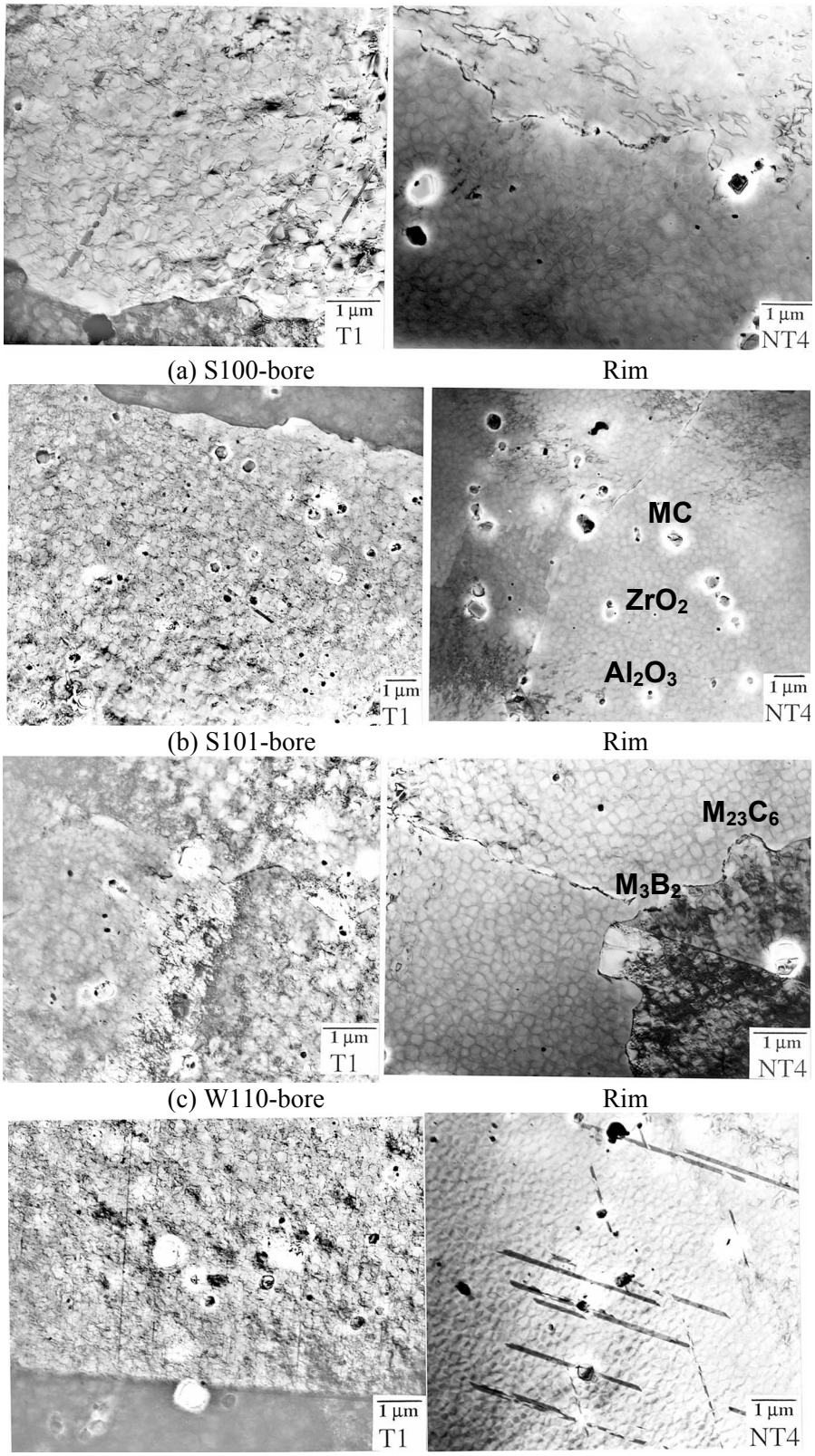

(a) S100-bore Rim

(b) S101-bore Rim

(c) W110-bore Rim

(d) H111-Bore Rim

Figure 5.—General microstructures and typical minor phases of bore (T1) and rim (NT4) specimens from supersolvus heat treated disks. (a) S100, (b) S101, (c) W110, (d) H111.

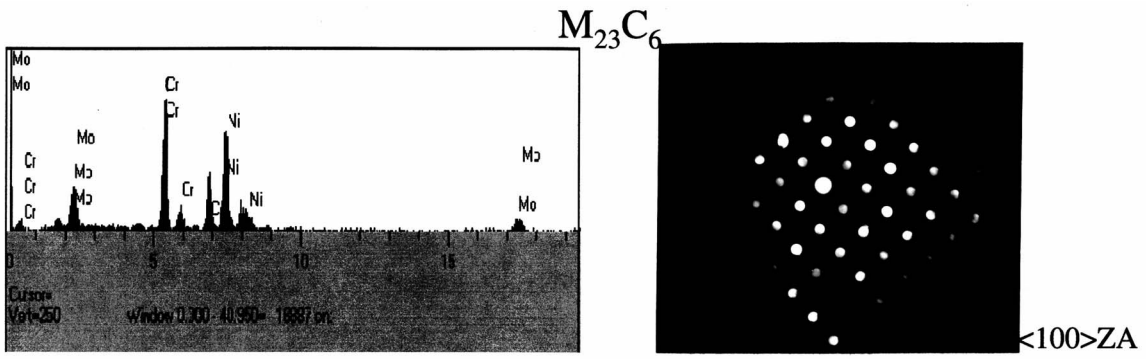

Figure 6.—Energy dispersive X-ray spectrum and selected area diffraction pattern of $M_{23}C_6$ carbides at grain boundaries, typical for all disks.

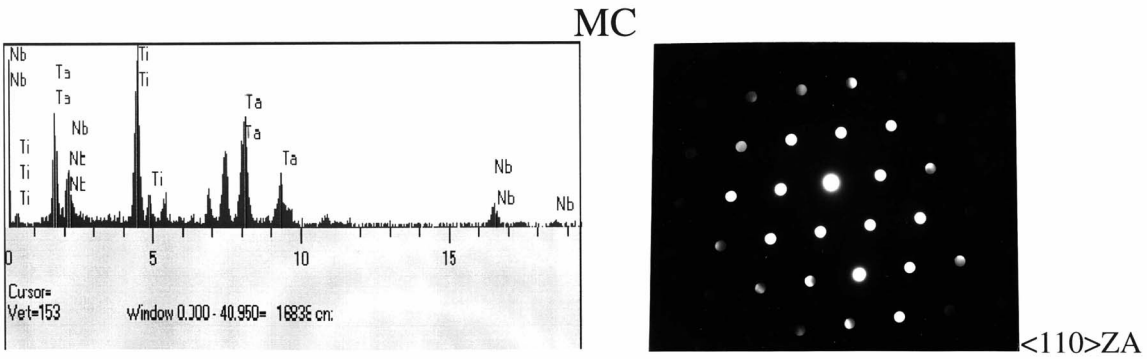

Figure 7.—Energy dispersive x-ray spectrum and selected area diffraction pattern of MC carbides within grains, typical for all disks.

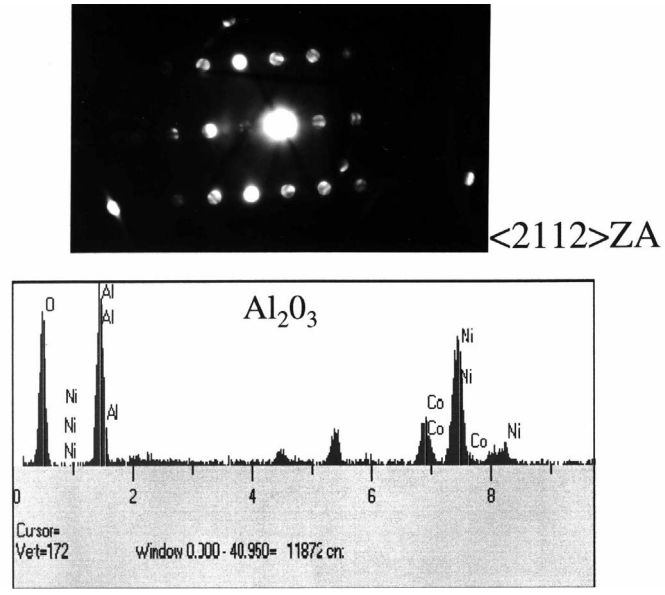

Figure 8.—Selected area diffraction pattern and energy dispersive x-ray spectrum of Al_2O_3 particle within grain, typical for all disks.

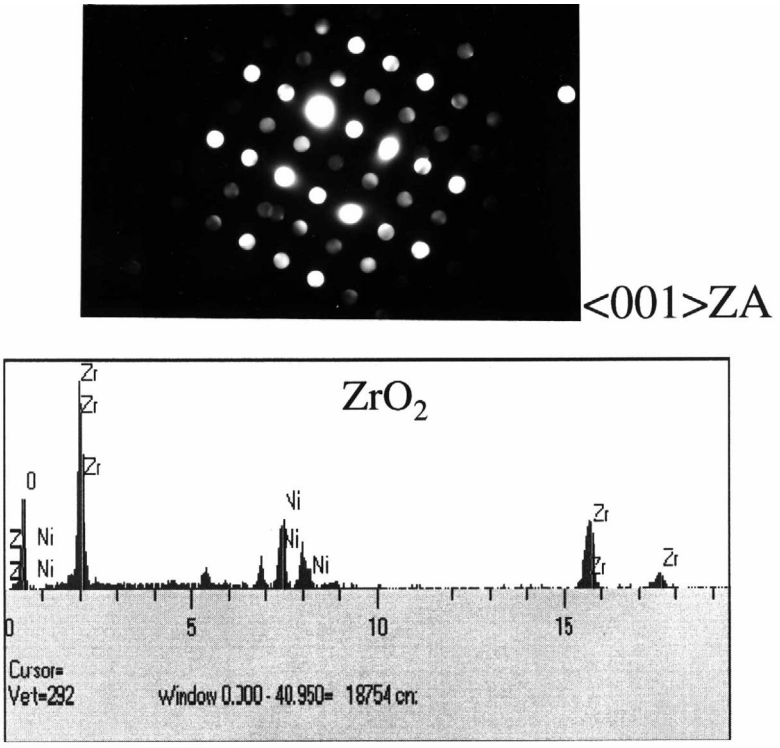

Figure 9.—Selected area diffraction pattern and energy dispersive x-ray spectrum of ZrO_2 particle within grain, typical for all disks.

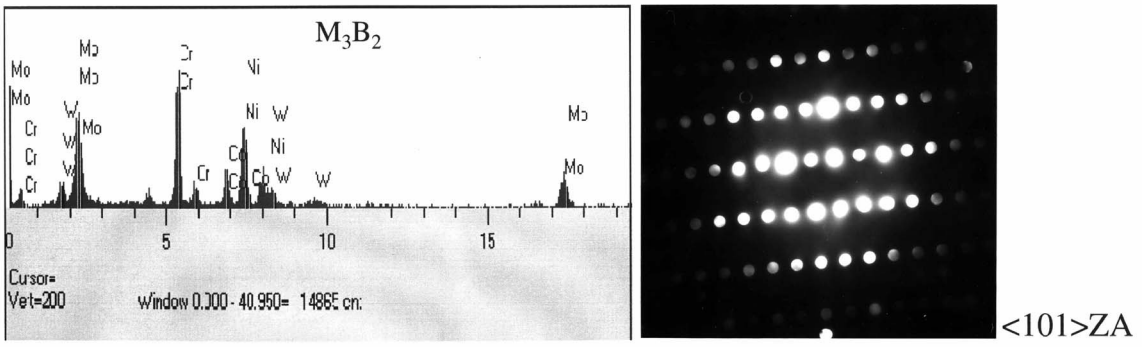

Figure 10.—Energy dispersive X-ray spectrum and selected area diffraction pattern of M_3B_2 particle at grain boundaries, typical for all disks.

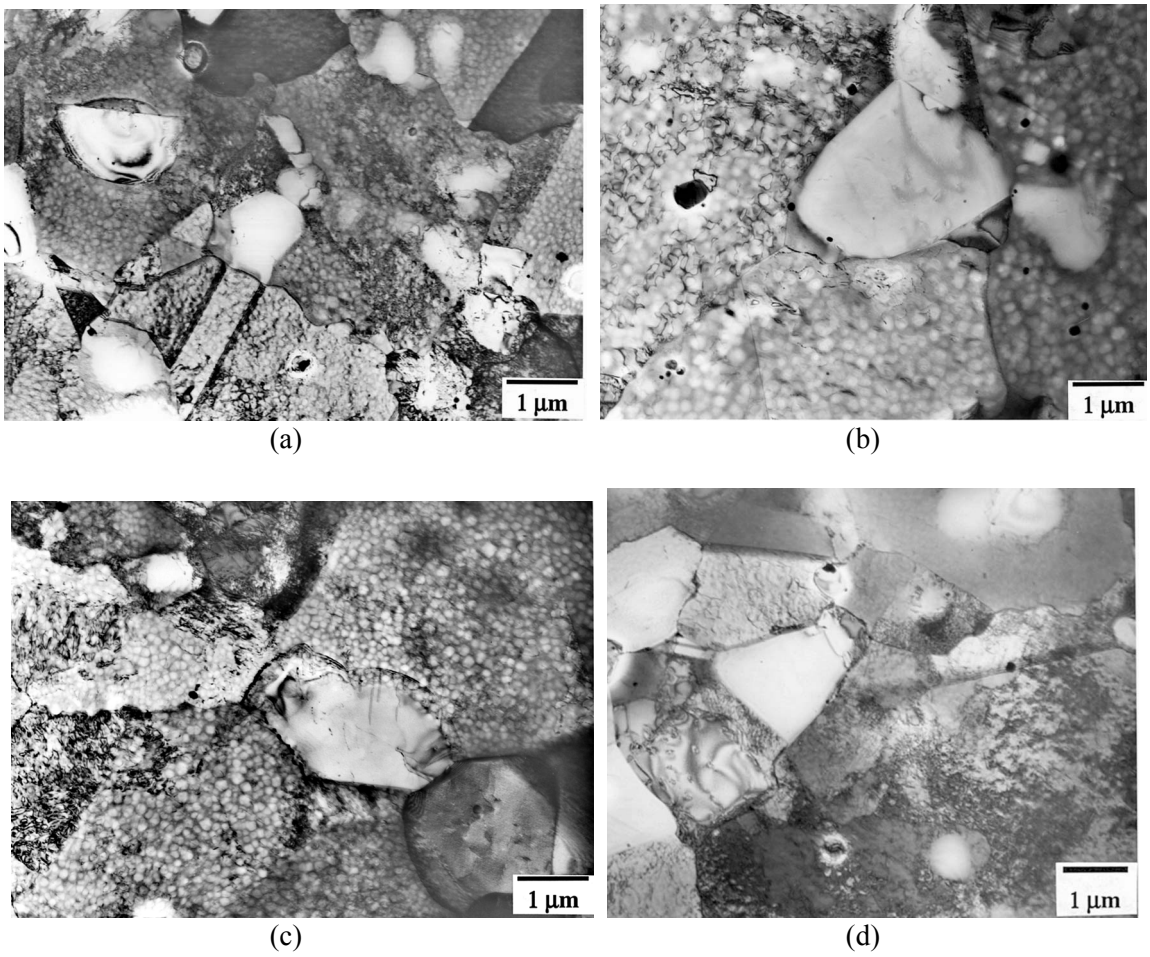

(a) (b)

(c) (d)

Figure 11.—General microstructures of rim (NT4) specimens from subsolvus heat treated disks. (a) W000, (b) S001, (c) S010, (d) W011.

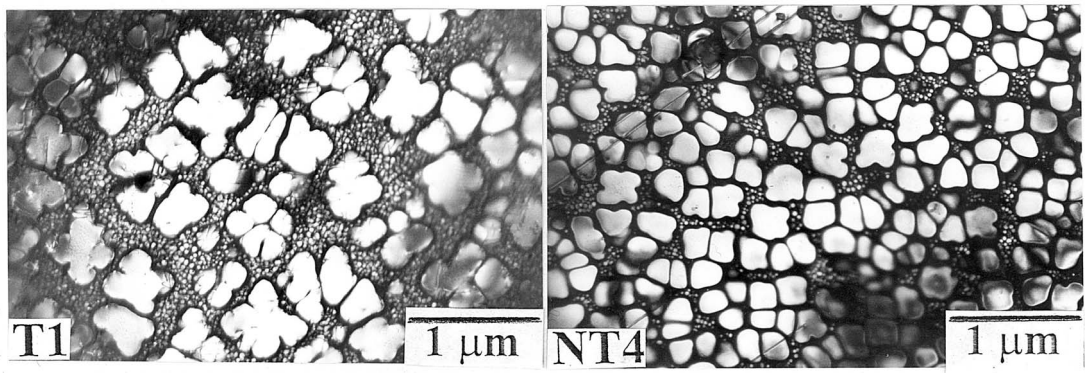

(a) S100-bore Rim

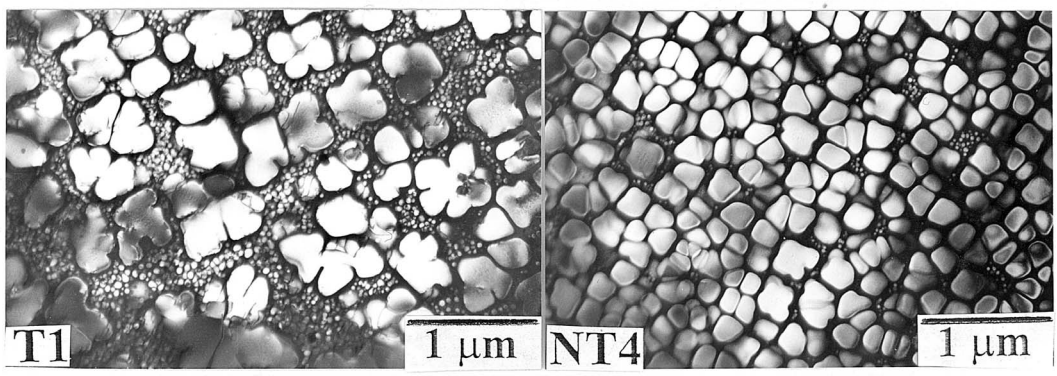

(b) S101-bore Rim

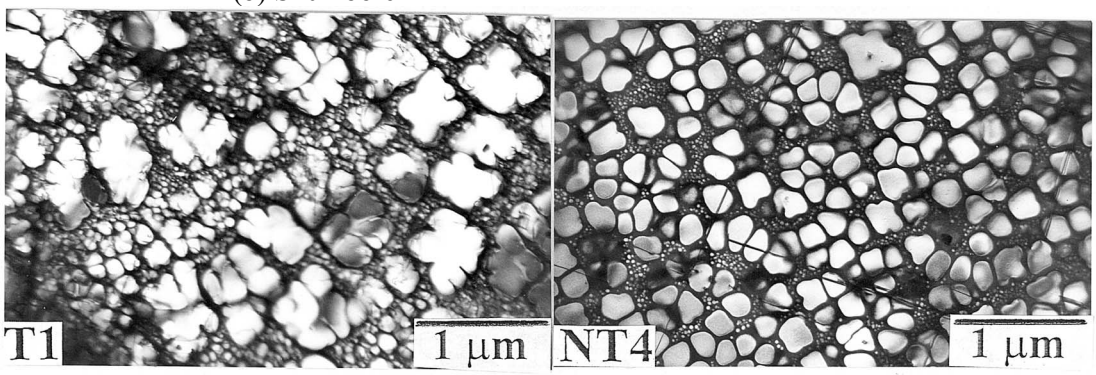

(c) W110-bore Rim

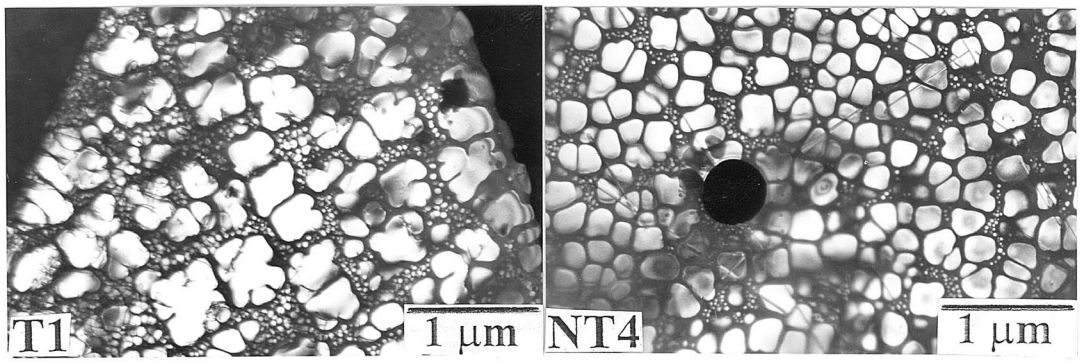

(d) H111-bore Rim

Figure 12.—γ′ microstructure within grains of bore (T1) and rim (NT4) specimens from supersolvus heat treated disks. (a) S100, (b) S101, (c) W110, (d) H111.

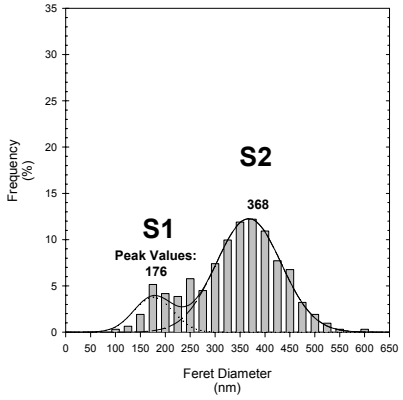

(a) S100-bore

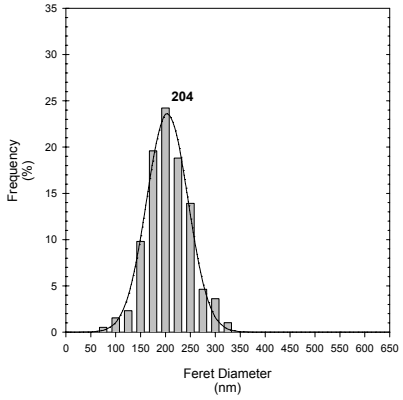

Rim

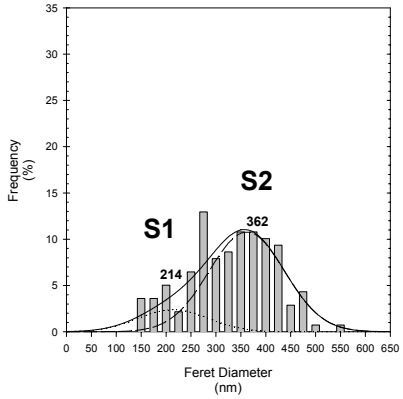

(b) S101-bore

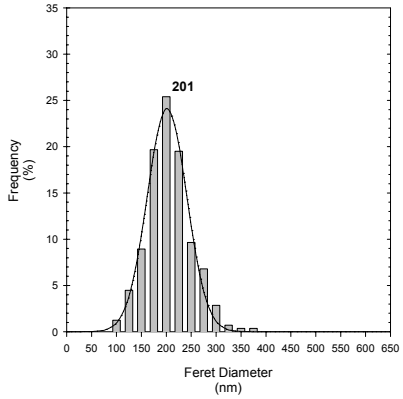

Rim

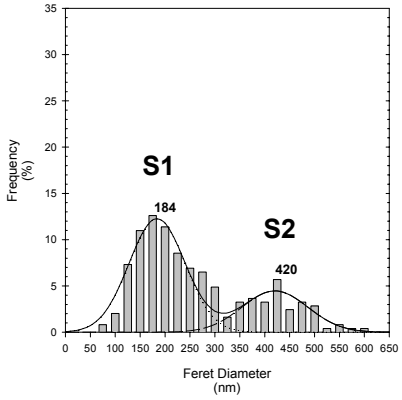

(c) W110-bore

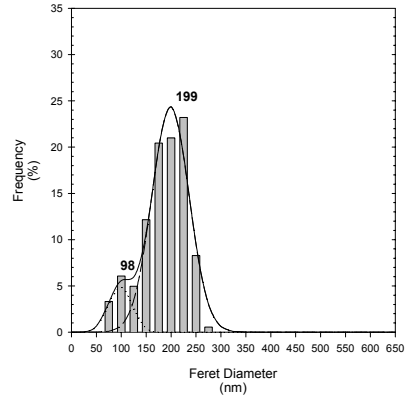

Rim

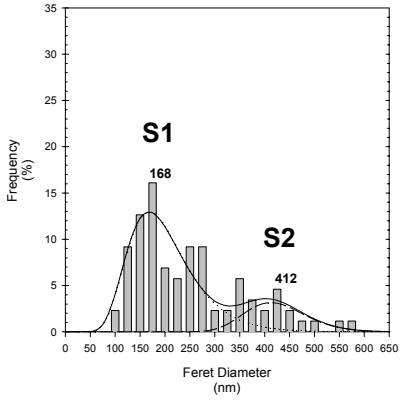

(d) H111-bore

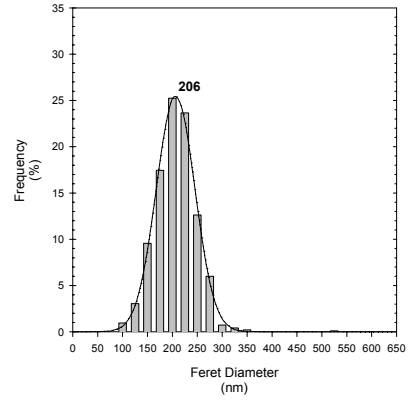

Rim

Figure 13.—Histograms of secondary γ′ feret diameters of bore (T1) and rim (NT4) specimens from disks. (a) S100, (b) S101, (c) W110, (d) H111.

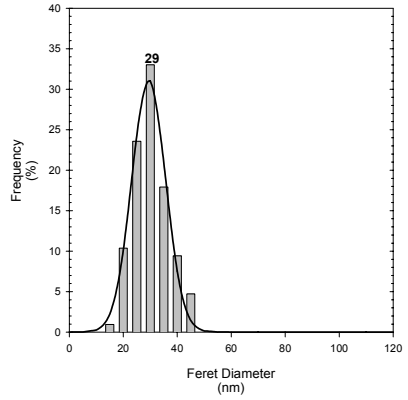

(a) S100-bore

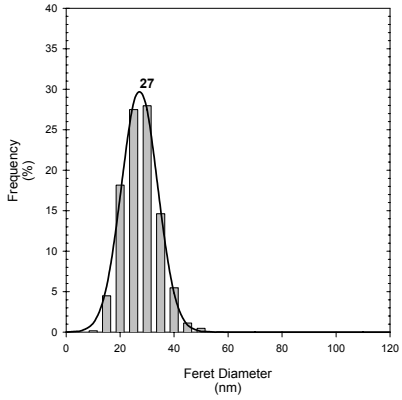

Rim

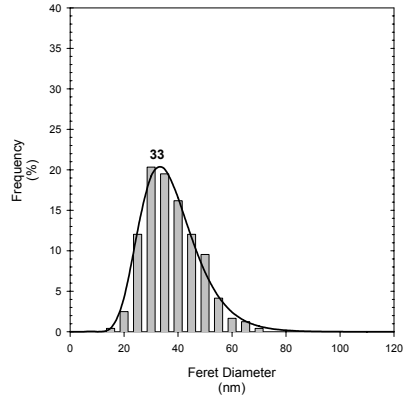

(b) S101-bore

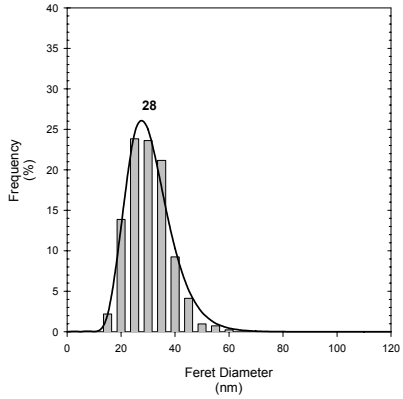

Rim

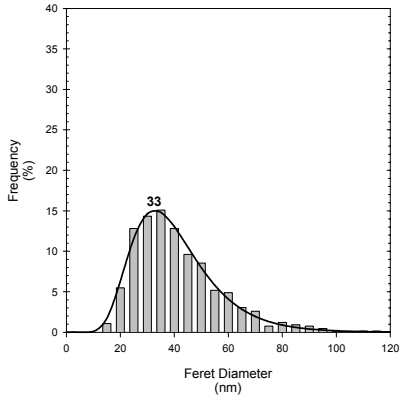

(c) W110-bore

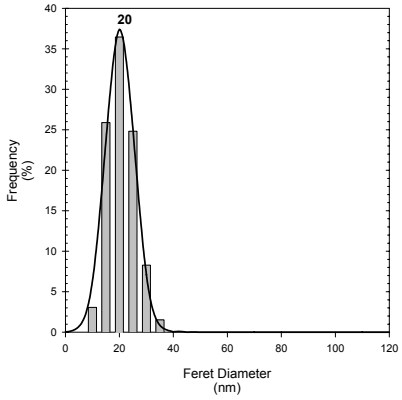

Rim

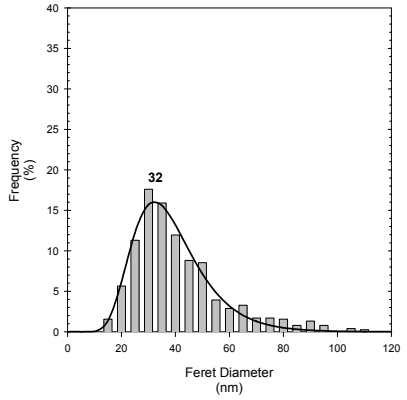

(d) H111-bore

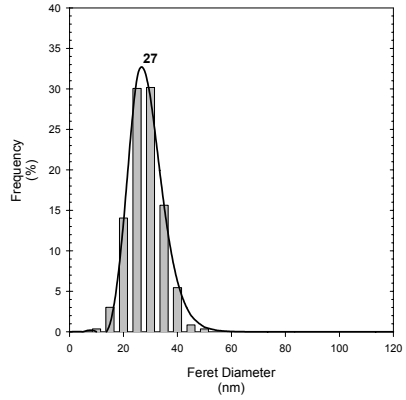

Rim

Figure 14.—Histograms of tertiary γ′ feret diameters of bore (T1) and rim (NT4) specimens from disks. (a) S100, (b) S101, (c) W110, (d) H111.

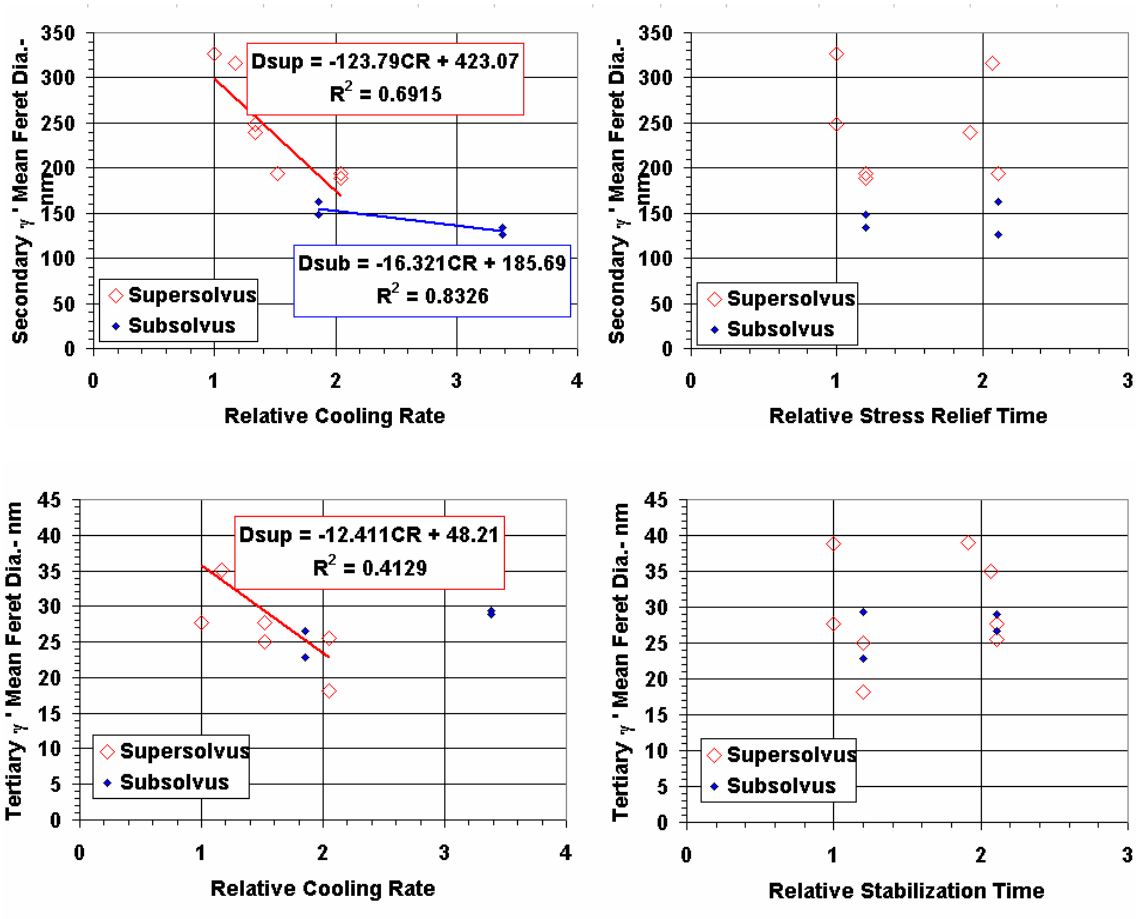

Figure 15.—Mean secondary and tertiary γ′ feret diameters versus relative cooling rate and stabilization time.

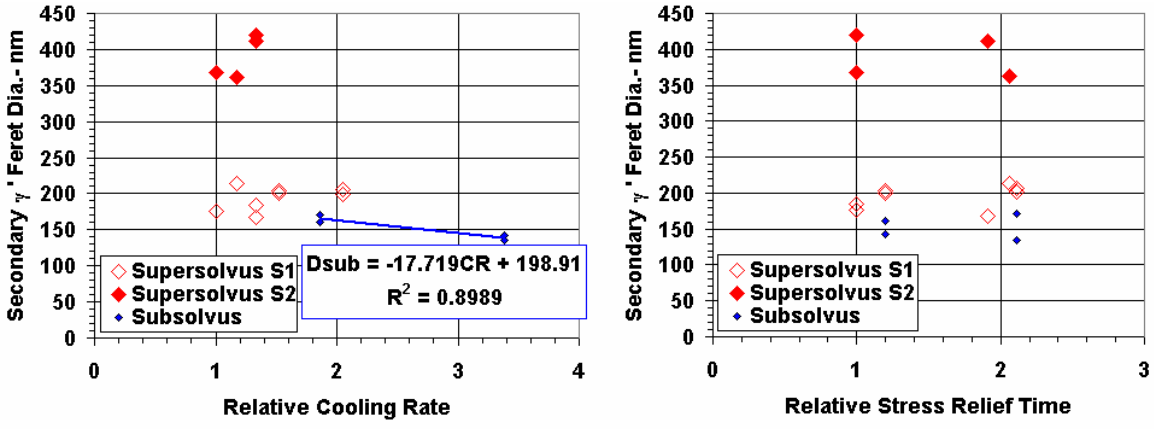

Figure 16.—Peaks from histograms for separated populations of secondary and tertiary γ′ feret diameters versus relative cooling rate and stabilization time.

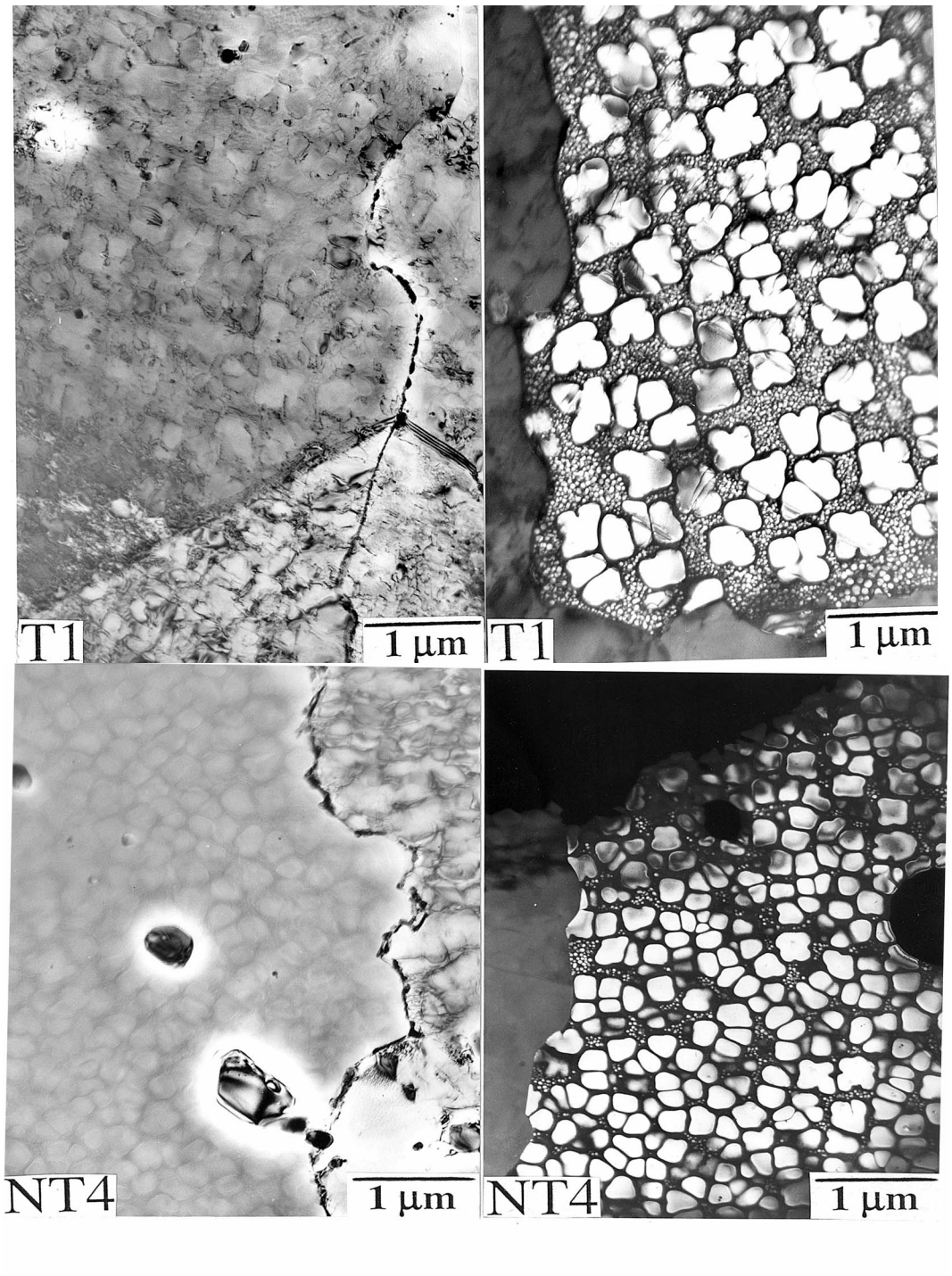

Figure 17.—Microstructure at grain boundaries of bore (T1) and rim (NT4) specimens from disk S100.

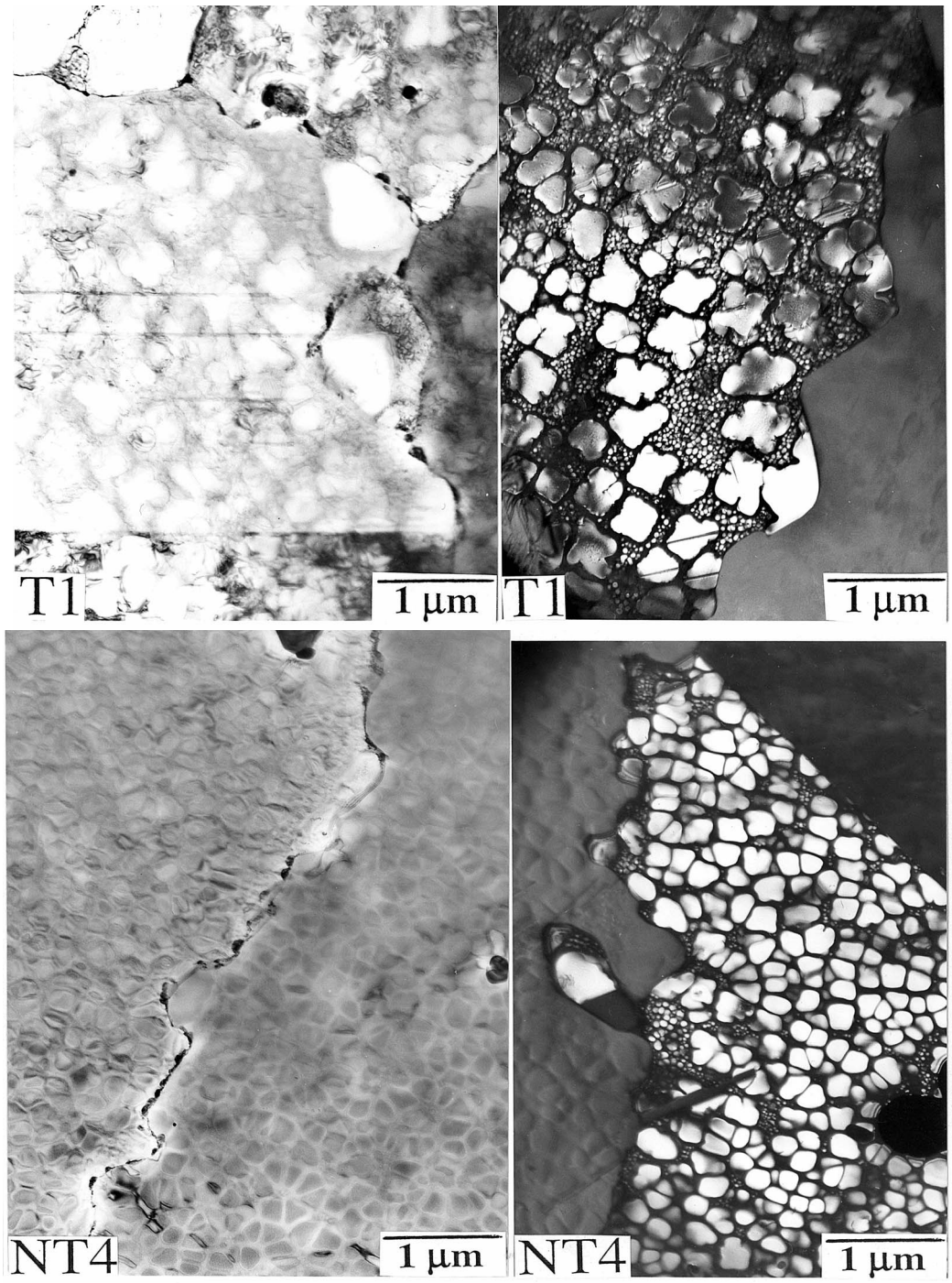

Figure 18.—Microstructure at grain boundaries of bore (T1) and rim (NT4) specimens from disk S101.

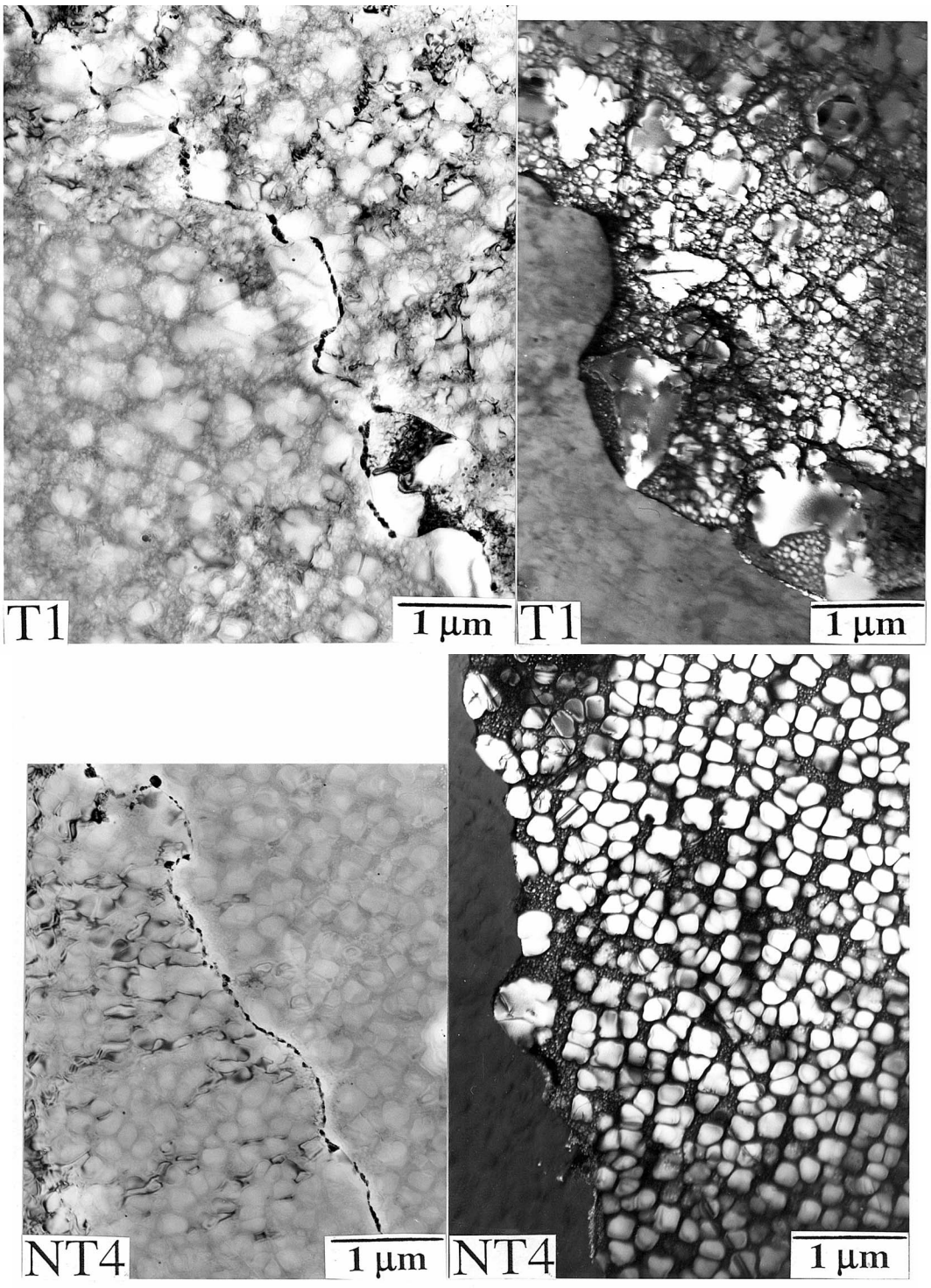

Figure 19.—Microstructure at grain boundaries of bore (T1) and rim (NT4) specimens from disk W110.

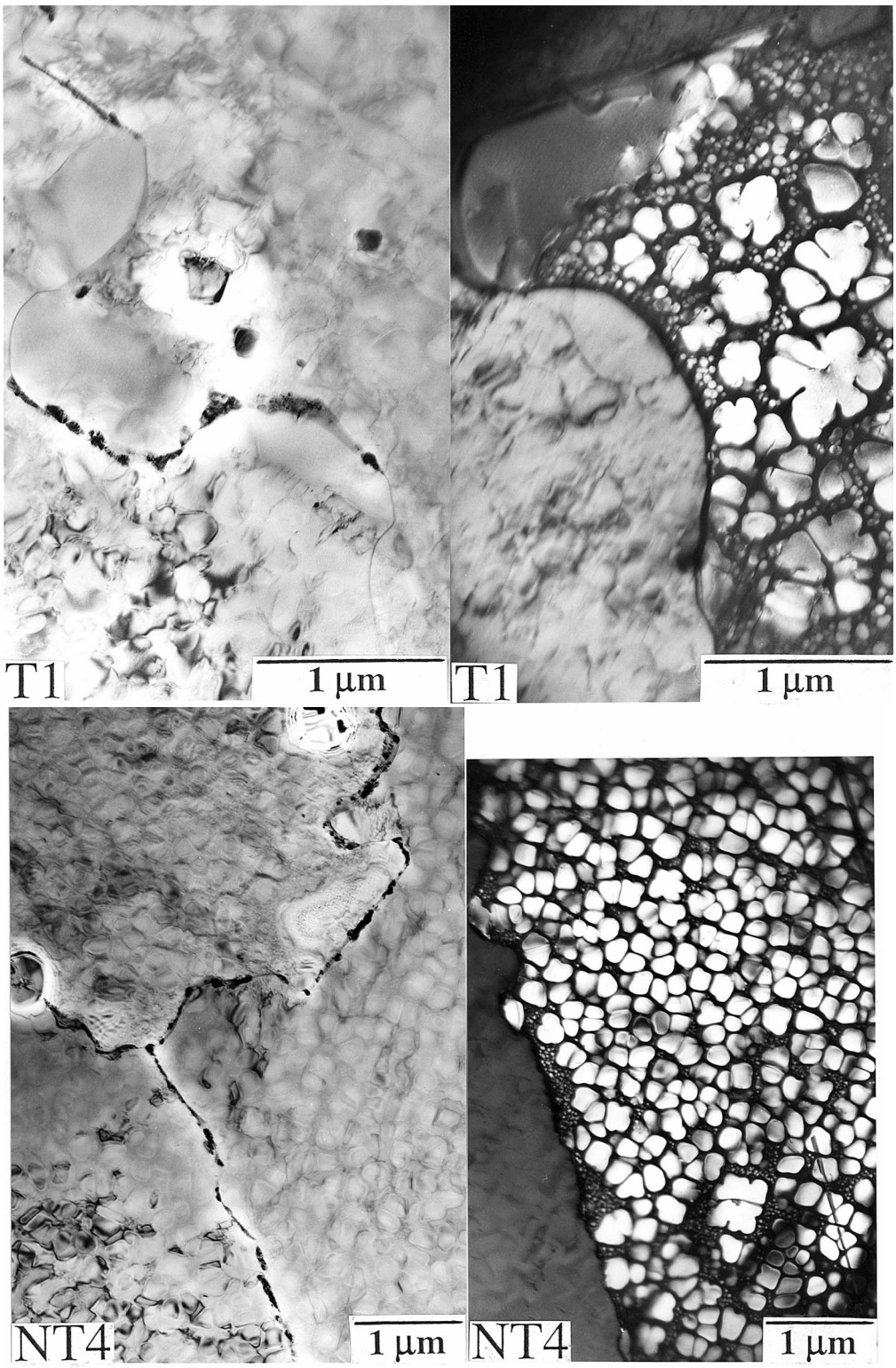

Figure 20.—Microstructure at grain boundaries of bore (T1) and rim (NT4) specimens from disk H111.

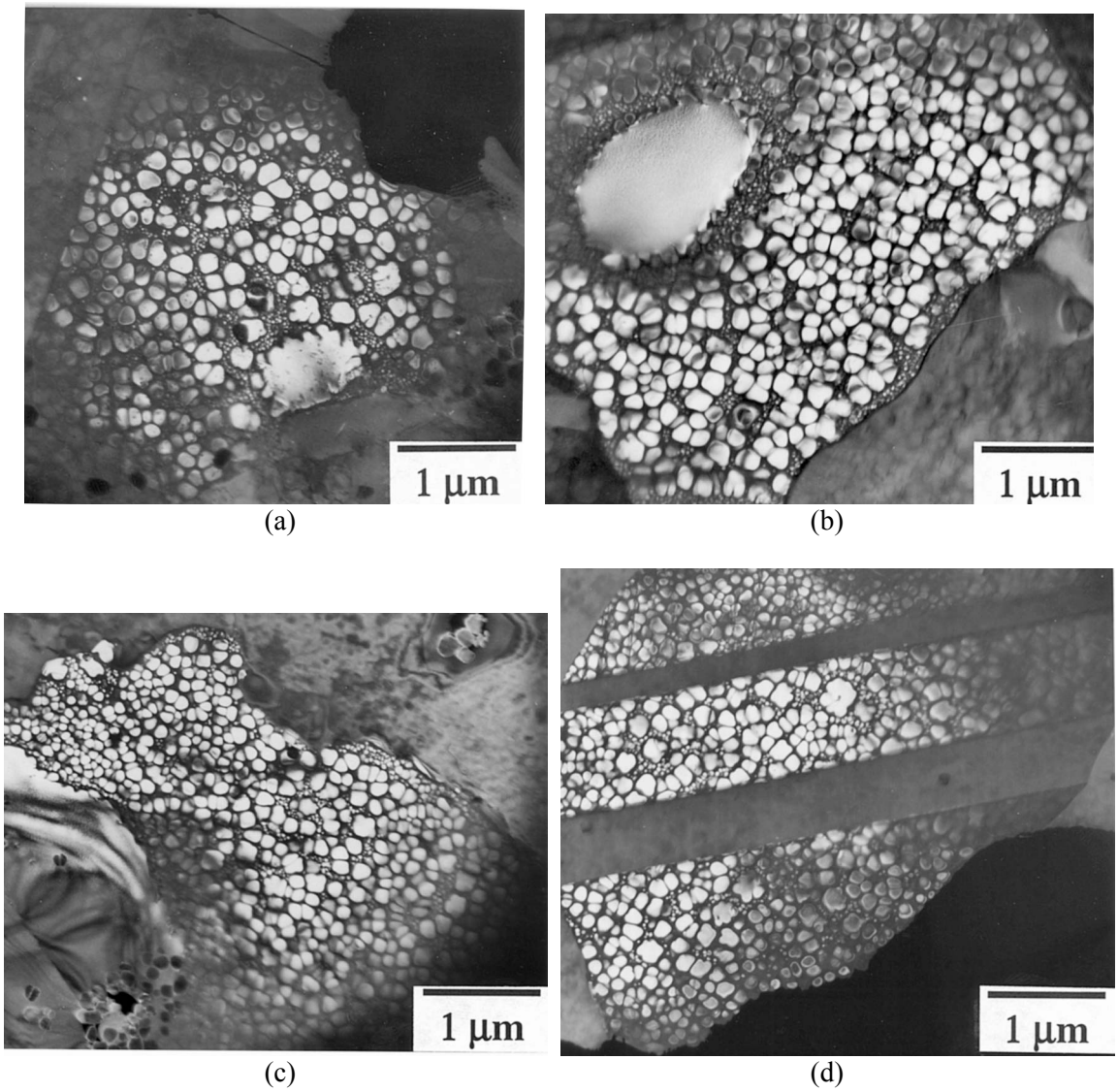

Figure 21.—γ′ microstructure within grains of rim specimens from subsolvus heat treated disks. (a) W000, (b) S001, (c) S010, (d) W011.

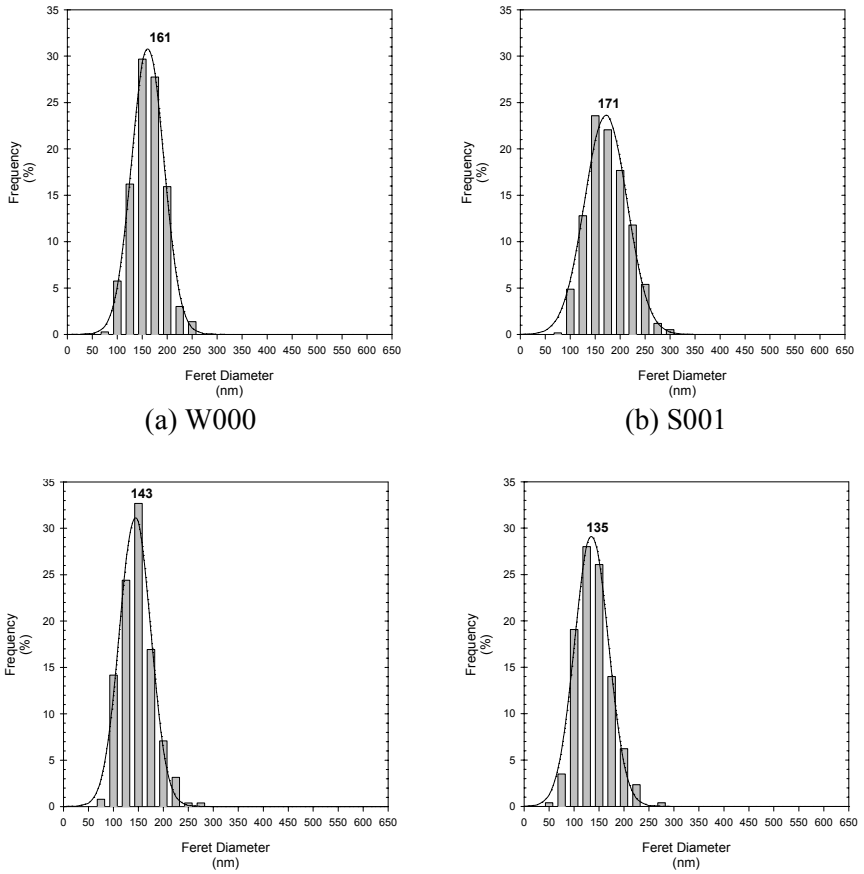

Figure 22.—Histograms of secondary γ′ feret diameters for rim specimens from subsolvus heat treated disks. (a) W000, (b) S001, (c) S010, (d) W011.

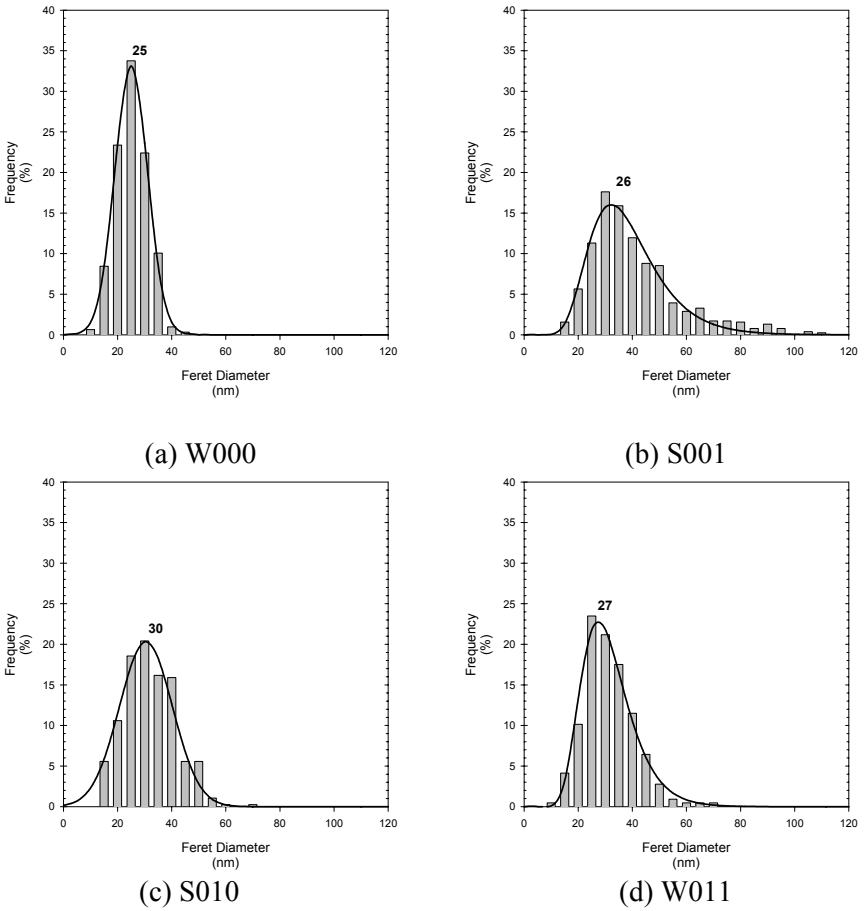

Figure 23.—Histograms of tertiary γ′ feret diameters for rim specimens from subsolvus heat treated disks. (a) W000, (b) S001, (c) S010, (d) W011.

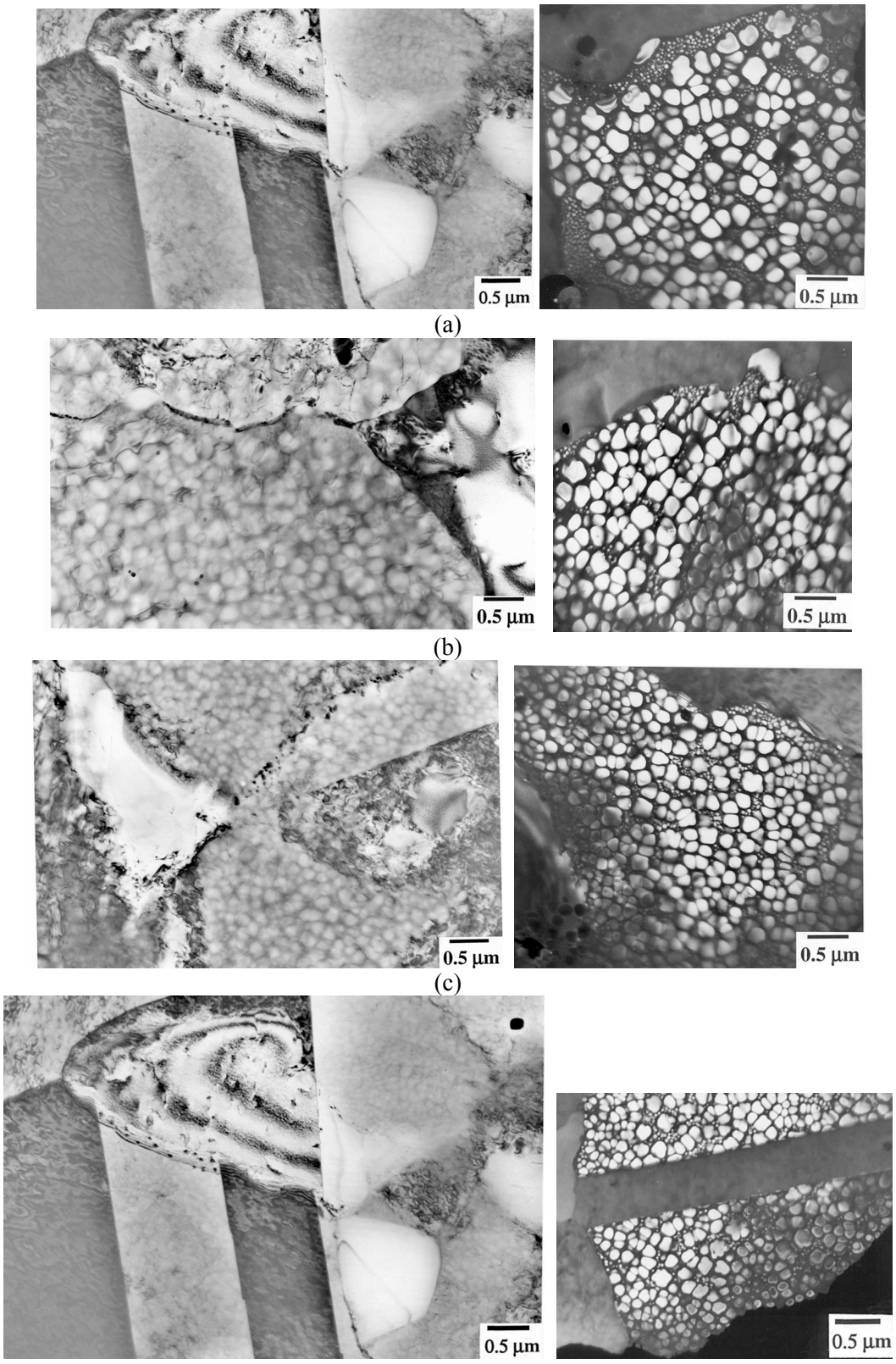

Figure 24.—Microstructure at grain boundaries for rim specimens of disks.
(a) W000, (b) S001, (c) S010, (d) W011.

REPORT DOCUMENTATION PAGE

Form Approved
OMB No. 0704-0188

1. AGENCY USE ONLY (*Leave blank*)	2. REPORT DATE	3. REPORT TYPE AND DATES COVERED
	May 2004	Technical Memorandum

4. TITLE AND SUBTITLE

Detailed Microstructural Characterization of the Disk Alloy ME3

5. FUNDING NUMBERS

WBS–22–714–30–05

6. AUTHOR(S)

Timothy P. Gabb, Anita Garg, David L. Ellis, and Kenneth M. O'Connor

7. PERFORMING ORGANIZATION NAME(S) AND ADDRESS(ES)

National Aeronautics and Space Administration
John H. Glenn Research Center at Lewis Field
Cleveland, Ohio 44135–3191

8. PERFORMING ORGANIZATION REPORT NUMBER

E–14533

9. SPONSORING/MONITORING AGENCY NAME(S) AND ADDRESS(ES)

National Aeronautics and Space Administration
Washington, DC 20546–0001

10. SPONSORING/MONITORING AGENCY REPORT NUMBER

NASA TM—2004–213066

11. SUPPLEMENTARY NOTES

Timothy P. Gabb, David L. Ellis, and Kenneth M. O'Connor, NASA Glenn Research Center; Anita Garg, University of Toledo, Toledo, Ohio 43606, and NASA Resident Research Associate at Glenn Research Center. Responsible person, Timothy P. Gabb, organization code 5120, 216–433–3272.

12a. DISTRIBUTION/AVAILABILITY STATEMENT

Unclassified - Unlimited
Subject Category: 07 Distribution: Nonstandard

Available electronically at http://gltrs.grc.nasa.gov

This publication is available from the NASA Center for AeroSpace Information, 301–621–0390.

12b. DISTRIBUTION CODE

13. ABSTRACT ***(Maximum 200 words)***

The advanced powder metallurgy disk alloy ME3 was designed using statistical screening and optimization of composition and processing variables in the NASA/General Electric/Pratt & Whitney HSR/EPM disk program to have extended durability for large disks at maximum temperatures of 600 to 700 °C. Scaled-up disks of this alloy were then produced at the conclusion of that program to demonstrate these properties in realistic disk shapes. The objective of the present study was to assess the microstructural characteristics of these ME3 disks at two consistent locations, in order to enable estimation of the variations in microstructure across each disk and across several disks of this advanced alloy. Scaled-up disks processed in the HSR/EPM Compressor/Turbine Disk program had been sectioned, machined into specimens, and tested in tensile, creep, fatigue, and fatigue crack growth tests by NASA Glenn Research Center, in cooperation with General Electric Engine Company and Pratt & Whitney Aircraft Engines. For this study, microstructures of grip sections from tensile specimens in the bore and rim were evaluated from these disks. The major and minor phases were identified and quantified using transmission electron microscopy (TEM). Particular attention was directed to the γ' precipitates, which along with grain size can predominantly control the mechanical properties of superalloy disks.

14. SUBJECT TERMS	15. NUMBER OF PAGES
Gas turbine engines; Superalloys; Disks; Precipitates; Grain size	42
	16. PRICE CODE

17. SECURITY CLASSIFICATION OF REPORT	18. SECURITY CLASSIFICATION OF THIS PAGE	19. SECURITY CLASSIFICATION OF ABSTRACT	20. LIMITATION OF ABSTRACT
Unclassified	Unclassified	Unclassified	